Available online at www.sciencedirect.com
SCIENCE DIRECT®
J. Non-Newtonian Fluid Mech. 117 (2004) 163–182
Journal of Non-Newtonian Fluid Mechanics
www.elsevier.com/locate/jnnfm

Stability of two-layer viscoelastic plane Couette flow past a deformable solid layer

V. Shankar*

Department of Chemical Engineering, Indian Institute of Technology, Kanpur 208016, India

Received 29 October 2003

Abstract

The stability of two-layer plane Couette flow of upper-convected Maxwell (UCM) fluids of thicknesses $(1-\beta)R$ and βR, with matched viscosities η, and relaxation times τ_1 and τ_2 past a soft, deformable solid layer (modeled here as a linear viscoelastic solid fixed to a rigid plate) of thickness HR, shear modulus G and viscosity η_w is determined using a temporal linear stability analysis in the creeping-flow regime where the inertia of the two fluids and the solid layer is negligible. Interfaces with and without the interfacial tension between the two fluids are considered, while the interfacial tension between the UCM fluid and the deformable solid is neglected. It is well known that the two-layer Couette flow of UCM fluids with different relaxation times undergoes a purely elastic interfacial instability (referred here as mode 1) in rigid-walled channels, even in the creeping flow limit. It was recently shown [J. Non-Newtonian Fluid Mech 116 (2004) 371] that the plane Couette flow of a *single* UCM fluid past a deformable solid layer also undergoes an instability (referred here as mode 2) in the creeping flow limit when the nondimensional solid elasticity parameter $\Gamma = V\eta/(GR)$ exceeds a certain critical value, for a given Weissenberg number $W = \tau V/R$. In this study, the respective effects of solid layer deformability and fluid elasticity stratification on mode 1 and mode 2, and the concomitant interaction of these two qualitatively different interfacial modes are analyzed in detail. It is shown that the deformability of the solid layer has a dramatic effect on the purely elastic (mode 1) interfacial instability between the two UCM fluids: When the more elastic UCM fluid is present in between the less elastic UCM fluid and the solid layer, the layer deformability has a stabilizing effect. In this configuration, if the thickness of the more elastic fluid is smaller than the less elastic fluid, it is shown that it is possible to *stabilize* the mode 1 purely elastic instability (except for very long and very short waves, the latter being stabilized usually by the nonzero interfacial tension between the two fluids) by making the solid layer sufficiently deformable (i.e., Γ exceeding a critical value), while such a configuration is *unstable* in the case of two-layer flow in rigid channels (i.e., in the absence of the deformable solid layer). Increase in the solid layer deformability, on the other hand, destabilizes the interfacial mode between the UCM fluid and the deformable solid (mode 2). It is demonstrated that it is possible to choose the solid elasticity parameter Γ and viscosity ratio η_w/η such that both mode 1 and mode 2 are completely stable in finite experimental geometries. In marked contrast, when the less elastic fluid is present in between the more elastic fluid and the solid layer, it is shown that solid layer deformability has a destabilizing effect on mode 1. For this configuration, if the thickness of the less elastic fluid is smaller, it is shown that mode 1 can be rendered *unstable* by increasing solid layer deformability, while it is *stable* in rigid channels (in the absence of the solid layer). In both of the above configurations, the nondimensional solid layer elasticity required respectively to stabilize or destabilize mode 1 varies as $\Gamma \propto (k^*R)^{-1}$ for $(k^*R) \ll 1$, where k^* is the wavenumber of perturbations. However, for finite experimental geometries the minimum allowed k^* is dictated by the system length, and in such cases, it is argued that complete stabilization or destabilization can be achieved for realistic values of Γ. In both the configurations, our results show that deformable solid layer coatings, by design or default, can completely suppress or induce purely elastic interfacial instabilities in two-layer flow of viscoelastic fluids past a deformable solid surface.

Keywords: Interfacial instability; Viscoelastic fluids; Two-layer flows; Linear stability analysis; Creeping flow

1. Introduction

The study of stability two-layer and three-layer flows of viscoelastic fluids is motivated in part by its relevance to polymer processing applications such as multilayer extrusion, where an accurate understanding of stable and unstable processing conditions can help in preventing interfacial

* Tel.: +91-512-259-7377.
E-mail address: vshankar@iitk.ac.in (V. Shankar).

0377-0257/$ – see front matter © 2004 Elsevier B.V. All rights reserved.
doi:10.1016/j.jnnfm.2004.01.009

Nomenclature

$c = c_r + ic_i$	complex wave-speed
G	shear modulus of the solid
H	nondimensional thickness of the solid
k	wavenumber
R	dimensional total thickness of the two fluids
V	dimensional velocity of the top plate
$W_\alpha = \tau_\alpha V/R$	Weissenberg number of fluid α
Greek letters	
β	nondimensional thickness of fluid 2
$(1-\beta)$	nondimensional thickness of fluid 1
$\Gamma = V\eta/(GR)$	nondimensional elasticity parameter of solid
η	viscosity of the two fluids
$\eta_r = \eta_w/\eta$	ratio of solid to fluid viscosity
η_w	viscosity of the solid layer
$\Sigma = \gamma^*/(\eta V)$	nondimensional fluid–fluid interfacial tension
τ_α	relaxation time of fluid α

instabilities which are detrimental to the quality of the final product. Apart from its practical relevance, the study of interfacial instabilities in two-layer and multilayer flows of viscoelastic fluids is also interesting from a fundamental view point, as viscoelastic fluids give rise to new mechanisms of interfacial instabilities that are absent in Newtonian fluids. Consequently, a large number of previous studies [1–8] (briefly discussed below) have focused on the theoretical understanding of two-layer and three-layer flows of viscoelastic fluids. These studies have clearly identified the parameter regimes in which interfacial instabilities occur, and have elucidated the physical mechanisms that underlie such instabilities in viscoelastic fluids. A series of experimental investigations on interfacial instabilities in the multilayer flow of viscoelastic fluids has been carried out by Wilson and Khomami [9–12]. A summary of the theoretical studies in this area can be found in Ganpule and Khomami [7].

In this paper, we consider the stability of the three-layer configuration consisting of a two-layer flow of viscoelastic fluids undergoing plane Couette flow past a soft, deformable solid layer (see Fig. 1). Such a configuration might be relevant in polymer processing where one may have a multilayer flow of polymeric liquids, in which each layer is being cross-linked to form a gel, possibly as part of a composite material. If one of the layers solidifies before the other, then the phenomena that are studied here could be relevant. One might also envision, in the case of a two-layer viscoelastic Couette flow, the use of soft solid layer coatings to manipulate and control the interfacial instabilities.

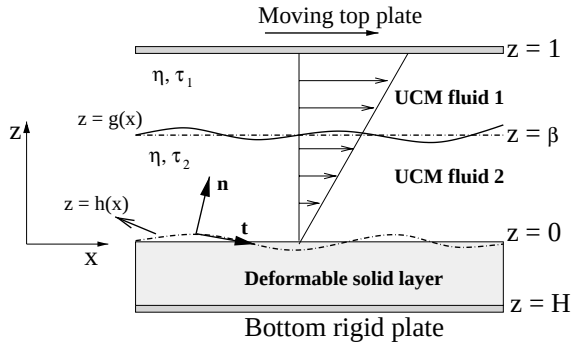

Fig. 1. Schematic diagram showing the configuration and (nondimensional) coordinate system considered in Section 2. Two UCM fluids with same viscosity η, but with different relaxation times τ_1 and τ_2 flowing past a deformable solid layer.

Indeed, there exists an extensive body of literature (for a recent overview, see, Gad-el-hak [13]) which have studied the stability of *Newtonian* fluid flow past compliant walls, in order to explore the possibility of delaying the onset of instabilities, and thereby achieve drag reduction at high Reynolds numbers. These studies have found, however, that while compliant walls may delay the boundary layer instability past rigid walls, they induce additional instabilities that arise due to the deformability of the wall. When a fluid flows past such soft solid layers, the dynamics of the fluid and the solid medium get coupled, and waves can propagate across the fluid–solid interface as the shear modulus of soft solids are in the range 10^3–10^6 Pa. An important question to be answered concerning the three-layer configuration of interest in the present study is whether the coupling between the dynamics of the fluid–solid interface and the two-fluid interface can result in suppression of interfacial instabilities in the two fluids. In this study, we explore this possibility of suppression of interfacial instabilities in the *creeping flow* limit where the inertia in the two fluids and the solid layer is neglected. In the remainder of this Introduction, relevant previous studies in the areas of multilayer flows of viscoelastic fluids in rigid channels and fluid flow past soft solid surfaces are briefly reviewed and the context and motivation for the present study are placed in perspective.

Yih [14] first showed using a longwave asymptotic analysis that the two-layer flow of Newtonian fluids of different viscosities is always stable in the absence of fluid inertia, while in the presence of even a vanishingly small Reynolds number, the interface becomes unstable due to viscosity stratification between the two fluids. However, for the case of two-layer Couette flow of upper-convected Maxwell (UCM) fluids, Chen [2] and Renardy [1], respectively, used long wave and short wave asymptotic analyses and showed that if the relaxation times of the two fluids are different, then the interface is unstable in the creeping flow limit even in the absence of viscosity differences between the two fluids. The discontinuity of the first normal stress difference in the base state between the two fluids was found

to be responsible for this interfacial instability. A number of subsequent studies [3–8] have examined the stability of two-layer and three-layer configurations of both Couette and plane Poiseuille flows of Oldroyd-B and UCM fluids using asymptotic and pseudospectral numerical methods. These studies have shown that when the thickness of the more elastic fluid is smaller than that of the less elastic fluid, the interface is unstable to perturbations with very long wavelengths, while for the converse case (viz. when the thickness of the more elastic fluid is larger) the interface is stable to perturbations of long and intermediate wavelengths.

A recent study by Shankar and Kumar [15] analyzed the stability of a *single* layer plane Couette flow of an UCM fluid past a deformable solid layer (modeled as a linear viscoelastic solid fixed to a rigid surface) in the creeping flow limit. This study showed that the interface between the UCM fluid and the solid becomes unstable when the solid layer becomes sufficiently deformable, i.e., when the parameter $\Gamma = V\eta/(GR)$ is *greater* than a critical value, and when the nondimensional group $\bar{W} = \tau G/\eta$ is *less* than a threshold value. Here, G is the shear modulus of the solid layer, η the viscosity of the fluid, V the velocity of the top wall driving the Couette flow, R the thickness of the fluid, and τ the relaxation time of the UCM fluid. The mechanism that drives this instability is the discontinuity of the base state velocity gradient at the fluid–solid interface, which couples the mean flow and the interfacial fluctuations even in the creeping flow limit via the tangential velocity condition at the fluid–solid interface. This is qualitatively different from the interfacial instability between two UCM fluids, which is driven by the discontinuity in the first normal stress difference at the interface.

For the three-layer configuration under consideration in this paper, there are two different interfacial modes, viz. the fluid–fluid interfacial mode, and the fluid–solid interfacial mode, both being unstable in the creeping flow limit due to qualitatively different mechanisms discussed above. We are interested in studying how these two qualitatively different interfacial modes interact with each other, and the consequences that this interaction has on the stability of the two modes. We use the upper-convected Maxwell model to represent the two viscoelastic fluids, as this model retains the essential physics necessary to capture the purely elastic interfacial instability between viscoelastic fluids. In order to isolate the central non-Newtonian aspect of the problem, we consider only the case where the viscosities of the two fluids are matched, while the relaxation times are different. A similar system was considered by Wilson and Rallison [5] for the case of three-layer superposed flow of Oldroyd-B liquids bounded by rigid walls. For the most part of this work, we use a simple linear viscoelastic model to describe the dynamics of the solid layer. In Section 3.4, we examine the consequence of using a neo-Hookean model for the solid layer, in order to determine whether the qualitative conclusions obtained using the linear viscoelastic model are affected by the use of a more complex constitutive relation for the solid layer.

The rest of this paper is organized as follows: The relevant governing equations and interface conditions are presented in Section 2.1, and the base state profiles are developed in Section 2.2. The linear stability analysis and the characteristic equation that determines the stability of the system under consideration are presented in Section 2.3. Representative results for the complex wavespeed as a function of the wavenumber, as well as neutral stability curves in appropriate parameter space are provided in Section 3. The salient results of our analysis as well as the limitations due to the assumptions of matched viscosities and creeping flow regime are discussed in the concluding Section 4.

2. Problem formulation

2.1. Governing equations

The system we consider (see Fig. 1) consists of a linear viscoelastic solid of thickness HR, shear modulus G, and viscosity η_w fixed onto a rigid surface at $z^* = -HR$, a layer of viscoelastic fluid (fluid 2) of thickness βR in the region $0 < z^* < \beta R$ with relaxation time τ_2, and another viscoelastic fluid layer (fluid 1) of thickness $(1-\beta)R$ in the region $\beta R < z^* < R$ with relaxation time τ_1. The two viscoelastic fluids are modeled using the UCM model (see, for example, [16]), which has two material constants: a constant viscosity η and a constant relaxation time τ. In this study, the viscosities of the two UCM fluids are assumed to be equal, while the relaxation times are different. In what follows, we indicate dimensional variables with a superscript $*$, and nondimensional variables without any superscript. Fluid 1 is bounded at $z^* = R$ by a rigid wall which moves at a constant velocity V in the x-direction relative to the deformable solid layer. It is useful to nondimensionalise various physical quantities at the outset, and the following scales are used for this purpose: R for lengths and displacements, V for velocities, R/V for time, and $\eta V/R$ for stresses and pressure. H, therefore, is the nondimensional thickness of the solid layer, while $(1-\beta)$ and β are, respectively, the nondimensional thickness of fluids 1 and 2.

The nondimensional equations governing the dynamics of the two fluids in the creeping-flow limit are, respectively, the continuity and momentum conservation equations:

$$\partial_i v^{(\alpha)} = 0, \quad \partial_j T_{ij}^{(\alpha)} = 0. \tag{1}$$

Here, $v^{(\alpha)}$ is the velocity field in fluid α ($\alpha = 1, 2$), and $T_{ij}^{(\alpha)}$ the total stress tensor in fluid α which is a sum of an isotropic pressure $-p_f^{(\alpha)}\delta_{ij}$ and the extra-stress tensor $\tau_{ij}^{(\alpha)}$:

$$T_{ij}^{(\alpha)} = -p_f^{(\alpha)}\delta_{ij} + \tau_{ij}^{(\alpha)}, \tag{2}$$

and the indices i, j take the values x, z. The extra-stress tensor is prescribed by the UCM constitutive relation as:

$$W_\alpha[\partial_t \tau_{ij}^{(\alpha)} + v_k^{(\alpha)}\partial_k \tau_{ij}^{(\alpha)} - \partial_k v_i^{(\alpha)} \tau_{kj}^{(\alpha)} - \partial_k v_j^{(\alpha)} \tau_{ki}^{(\alpha)}] + \tau_{ij}^{(\alpha)} = (\partial_i v_j^{(\alpha)} + \partial_j v_i^{(\alpha)}), \quad (3)$$

where $\partial_t \equiv (\partial/\partial t)$, $\partial_i \equiv (\partial/\partial x_i)$, and $W_\alpha = \tau_\alpha V/R$ is the Weissenberg number in fluid α. No-slip boundary conditions are appropriate for fluid 1 at $z = 1$:

$$v_x^{(1)} = 1, \quad v_z^{(1)} = 0, \quad (4)$$

while the boundary conditions at the interface between the two UCM fluids and the interface between the fluid and the solid layer are discussed below.

The deformable solid layer is modeled as an incompressible linear viscoelastic solid, similar to that used in the previous studies in this area (see, for example, [15,17–20]). The dynamics of the solid layer is described by a displacement field u_i, which represents the displacement of the material points in the medium from their steady-state positions. The velocity field in the solid layer is $v_i = \partial_t u_i$. In an incompressible linear viscoelastic solid, the displacement field satisfies the continuity equation:

$$\partial_i u_i = 0. \quad (5)$$

The momentum conservation equation, in the limit where the inertial stresses in the solid layer are negligible, is given by:

$$\partial_j \Pi_{ij} = 0, \quad (6)$$

where $\Pi_{ij} = -p_g \delta_{ij} + \sigma_{ij}$ is the total stress tensor which is given by a sum of the isotropic pressure p_g and deviatoric stress σ_{ij}. The neglect of inertial stresses in the solid requires that the density of the solid layer is comparable to the density of the fluid. The deviatoric stress tensor σ_{ij} is given by a sum of elastic and viscous stresses in the solid layer:

$$\sigma_{ij} = \left(\frac{1}{\Gamma} + \eta_r \partial_t\right)(\partial_i u_j + \partial_j u_i), \quad (7)$$

where $\Gamma = V\eta/(GR)$ is the nondimensional quantity characterizing the elasticity of the solid layer and $\eta_r = \eta_w/\eta$ the ratio of solid to fluid viscosities. More precisely, $1/\Gamma$ is the estimated ratio of elastic stresses in the solid layer to viscous stresses in the UCM fluids. The solid layer is assumed to be fixed to a rigid surface at $z = -H$, and the boundary condition for the displacement field there is $u_i = 0$.

A recent study by Gkanis and Kumar [21] (also see [15]) on the stability of the plane Couette flow of a Newtonian fluid past a deformable solid has examined the role of nonlinear rheological properties in the solid by modeling the deformable solid using the neo-Hookean model. This study shows that for nonzero interfacial tension between the fluid and the solid medium, and sufficiently large values of solid layer thickness ($H \geq 2$), the results from both linear and nonlinear solid models agree quite well, while for smaller values of solid thickness, the linear model somewhat overpredicts the critical velocity required for destabilizing the flow. In addition, there appears one more unstable mode in the high wavenumber range in the neo-Hookean model, and for $H < 2$, the critical value of $\Gamma = V\eta/(GR)$ required to destabilize the flow is smaller for this high wavenumber instability. In Section 3.4, we present a few representative comparisons of the neutral stability curves obtained from the linear viscoelastic model as well as the neo-Hookean model for the solid layer, in order to demonstrate that the linear viscoelastic solid model yields qualitatively correct results for the present problem.

The conditions at the interface $z = g(x)$ between the two UCM fluids are the continuity of the velocities and stresses, and the kinematic condition for the evolution of the interfacial position $g(x)$. The conditions at the interface $z = h(x)$ between UCM fluid 2 and the solid layer are the continuity of the velocities and stresses. We neglect the effect of interfacial tension between UCM fluid 2 and the solid layer, as this was found in an earlier study [17] to have a purely stabilizing effect on the interfacial mode of the interface at $z = h(x)$ between the fluid and the solid layer.

2.2. Base state

The steady velocity profile is simply the Couette flow profile throughout the two fluids, identical to that found for Newtonian fluids:

$$\bar{v}_x^{(1)} = z, \quad \bar{v}_z^{(1)} = 0, \quad \bar{\tau}_{xx}^{(1)} = 2W_1, \quad \bar{\tau}_{zz}^{(1)} = 0, \quad \bar{\tau}_{xz}^{(1)} = \bar{\tau}_{zx}^{(1)} = 1, \quad (8)$$

$$\bar{v}_x^{(2)} = z, \quad \bar{v}_z^{(2)} = 0, \quad \bar{\tau}_{xx}^{(2)} = 2W_2, \quad \bar{\tau}_{zz}^{(2)} = 0, \quad \bar{\tau}_{xz}^{(2)} = \bar{\tau}_{zx}^{(2)} = 1. \quad (9)$$

Since the viscosities of the two UCM fluids are equal, the gradient of the velocity profile in the two fluids is identical. Note, however, that the nonzero first normal stress difference $\bar{\tau}_{xx}^{(\alpha)} - \bar{\tau}_{zz}^{(\alpha)} = 2W_\alpha$, $(\alpha = 1, 2)$ is different in the two fluids, and it is discontinuous across the two-fluid interface. The solid layer is at rest in this steady base state, but there is a nonzero unidirectional displacement $\bar{u}_x$ due to the fluid shear stresses at the interface:

$$\bar{u}_x = \Gamma(z + H), \quad \bar{u}_z = 0, \quad \bar{\sigma}_{xx} = 0, \quad \bar{\sigma}_{zz} = 0, \quad \bar{\sigma}_{xz} = \bar{\sigma}_{zx} = 1. \quad (10)$$

All the base flow quantities above are denoted with an overbar in the preceding and ensuing discussions.

2.3. Linear stability analysis

Small perturbations (denoted by primed quantities) are introduced to the fluid velocity about the base state, $v_i^{(\alpha)} = \bar{v}_i^{(\alpha)} + v_i^{(\alpha)'}$, and other dynamical quantities in the two fluids and the solid layer are similarly perturbed. We use a temporal stability analysis to determine the fate of small perturbations to the above base state. All the perturbation quantities are expanded in the form of spatially periodic Fourier modes

in the x-direction, and with an exponential dependence on time:

$$v_i^{(\alpha)'} = \tilde{v}_i^{(\alpha)'}(z)\exp[\mathrm{i}k(x-ct)],$$
$$u_i' = \tilde{u}_i(z)\exp[\mathrm{i}k(x-ct)], \quad \alpha = 1, 2, \tag{11}$$

where k is the wavenumber, c the wavespeed which is a complex number, and $\tilde{v}_i^{(\alpha)}(z)$ and $\tilde{u}_i^{(\alpha)}(z)$ are eigenfunctions which are determined below from the linearized governing equations and boundary conditions. For simplicity, only two-dimensional perturbations are considered. The complex wavespeed is $c = c_\mathrm{r} + \mathrm{i}c_\mathrm{i}$, and when $c_\mathrm{i} > 0$, the base state is temporally unstable.

Upon substituting the above form for the perturbations in the governing equations for the two fluids (1) and the constitutive relation for the two UCM fluids (3), we obtain the following linearized equations for the two fluids, where $\alpha = 1, 2$ and $\mathrm{d}_z = \mathrm{d}/\mathrm{d}z$:

$$\mathrm{d}_z\tilde{v}_z^{(\alpha)} + \mathrm{i}k\tilde{v}_x^{(\alpha)} = 0, \tag{12}$$

$$-\mathrm{i}k\tilde{p}_f^{(\alpha)} + \mathrm{i}k\tilde{\tau}_{xx}^{(\alpha)} + \mathrm{d}_z\tilde{\tau}_{xz}^{(\alpha)} = 0, \tag{13}$$

$$-\mathrm{d}_z\tilde{p}_f^{(\alpha)} + \mathrm{d}_z\tilde{\tau}_{zz}^{(\alpha)} + \mathrm{i}k\tilde{\tau}_{xz}^{(\alpha)} = 0, \tag{14}$$

$$\{1 + \mathrm{i}kW_\alpha(z-c)\}\tilde{\tau}_{zz}^{(\alpha)} = 2\mathrm{d}_z\tilde{v}_z^{(\alpha)} + 2\mathrm{i}kW_\alpha\tilde{v}_z^{(\alpha)}, \tag{15}$$

$$\{1 + \mathrm{i}kW_\alpha(z-c)\}\tilde{\tau}_{xz}^{(\alpha)} = (\mathrm{d}_z\tilde{v}_x^{(\alpha)} + \mathrm{i}k\tilde{v}_z^{(\alpha)}) + W_\alpha(\tilde{\tau}_{zz}^{(\alpha)} + 2\mathrm{i}kW_\alpha\tilde{v}_z^{(\alpha)}), \tag{16}$$

$$\{1 + \mathrm{i}kW_\alpha(z-c)\}\tilde{\tau}_{xx}^{(\alpha)} = 2\mathrm{i}k\tilde{v}_x^{(\alpha)} + W_\alpha(2\tilde{\tau}_{xz}^{(\alpha)} + 4\mathrm{i}kW_\alpha\tilde{v}_x^{(\alpha)} + 2\mathrm{d}_z\tilde{v}_x^{(\alpha)}). \tag{17}$$

The above equations can be reduced to a single fourth-order equation for $\tilde{v}_z$ [22]:

$$\{\xi_\alpha^2\mathrm{d}_z^2 - 2\xi_\alpha\mathrm{d}_z + 2 - k^2\xi_\alpha^2\}\{\mathrm{d}_z^2 + 2\mathrm{i}kW_\alpha\mathrm{d}_z - k^2 - 2k^2W_\alpha^2\}\tilde{v}_z^{(\alpha)} = 0, \tag{18}$$

where the variable ξ_α is defined as $\xi_\alpha = [z - c - \mathrm{i}/(kW_\alpha)]$, $\alpha = 1, 2$.

The governing equations for the displacement field in the solid layer can be expressed in terms of $\tilde{u}_i(z)$ in a similar manner to give:

$$\mathrm{d}_z\tilde{u}_z + \mathrm{i}k\tilde{u}_x = 0, \tag{19}$$

$$-\mathrm{i}k\tilde{p}_g + \left(\frac{1}{\Gamma} - \mathrm{i}kc\eta_\mathrm{r}\right)(\mathrm{d}_z^2 - k^2)\tilde{u}_x = 0, \tag{20}$$

$$-\mathrm{d}_z\tilde{p}_g + \left(\frac{1}{\Gamma} - \mathrm{i}kc\eta_\mathrm{r}\right)(\mathrm{d}_z^2 - k^2)\tilde{u}_z = 0. \tag{21}$$

These equations can be reduced to a single fourth-order differential equation for $\tilde{u}_z$:

$$(\mathrm{d}_z^2 - k^2)(\mathrm{d}_z^2 - k^2)\tilde{u}_z = 0. \tag{22}$$

The linearized boundary conditions at the unperturbed interface position $z = 0$ between UCM fluid 2 and the solid layer are given by [15]:

$$\tilde{v}_z^{(2)} = (-\mathrm{i}kc)\tilde{u}_z, \tag{23}$$

$$\tilde{v}_x^{(2)} + \tilde{u}_z = (-\mathrm{i}kc)\tilde{u}_x, \tag{24}$$

$$-\tilde{p}_f^{(2)} + \tilde{\tau}_{zz}^{(2)} = -\tilde{p}_g + \frac{1}{\Gamma}2\mathrm{d}_z\tilde{u}_z - 2\mathrm{i}kc\eta_\mathrm{r}\mathrm{d}_z\tilde{u}_z, \tag{25}$$

$$\tilde{\tau}_{xz}^{(2)} - 2\mathrm{i}kW_2\tilde{u}_z = \left(\frac{1}{\Gamma} - \mathrm{i}kc\eta_\mathrm{r}\right)(\mathrm{d}_z\tilde{u}_x + \mathrm{i}k\tilde{u}_z). \tag{26}$$

Here, the second term in the left side of Eqs. (24) and (26) represent nontrivial contributions that arise as a result of the Taylor expansion of the mean flow quantities about the unperturbed fluid–solid interface. The additional term that appears in Eq. (24) for the tangential velocity is responsible for the instability of the interface between the fluid and the deformable solid layer [15,17].

Similarly, the linearized boundary conditions at the unperturbed interface position $z = \beta$ between the two UCM fluids 1 and 2 are given by:

$$\tilde{v}_z^{(1)} = \tilde{v}_z^{(2)}, \tag{27}$$

$$\tilde{v}_x^{(1)} = \tilde{v}_x^{(2)}, \tag{28}$$

$$-\tilde{p}_f^{(1)} + \tilde{\tau}_{zz}^{(1)} - \Sigma k^2\tilde{g} = -\tilde{p}_f^{(2)} + \tilde{\tau}_{zz}^{(2)} \tag{29}$$

$$\tilde{\tau}_{xz}^{(1)} - 2\mathrm{i}kW_1\tilde{g} = \tilde{\tau}_{xz}^{(2)} - 2\mathrm{i}kW_2\tilde{g}, \tag{30}$$

where $\tilde{g}$ is the Fourier expansion coefficient for the interface position $g = \tilde{g}\exp[\mathrm{i}k(x-ct)]$, and $\Sigma = \gamma^*/(\eta V)$ the nondimensional interfacial tension between UCM fluids 1 and 2. Note that in the tangential velocity condition (Eq. (28)), there are no additional terms that arise due to Taylor expansion, because in the base state both the fluid velocity and the velocity gradient are continuous across the two-fluid interface (owing to matched viscosities in fluids 1 and 2). The tangential stress condition (Eq. (30)) has additional terms due to the jump in the first normal stress difference across the two-fluid interface in the base state. These additional terms are responsible for the purely elastic interfacial instability in two-layer flows of UCM fluids. The linearized kinematic condition at $z = \beta$ between the two UCM fluids is given by

$$\mathrm{i}k(\beta - c)\tilde{g} = \tilde{v}_z^{(1)}[z = \beta]. \tag{31}$$

The boundary conditions at $z = 1$ are simply $\tilde{v}_z^{(1)} = 0$ and $\tilde{v}_x^{(1)} = 0$, while the boundary conditions at $z = -H$ are $\tilde{u}_z = 0$ and $\tilde{u}_x = 0$.

The general solution to the fourth-order differential equation governing the stability of the two UCM fluids (18) can be obtained analytically, following Gorodtsov and Leonov [22]:

$$\tilde{v}_z^{(1)} = A_1(z-c)\exp[kz] + A_2(z-c)\exp[-kz] + A_3\exp[k(-\mathrm{i}W_1 + \sqrt{1+W_1^2})z] + A_4\exp[-k(\mathrm{i}W_1 + \sqrt{1+W_1^2})z], \quad (32)$$

$$\tilde{v}_z^{(2)} = B_1(z-c)\exp[kz] + B_2(z-c)\exp[-kz] + B_3\exp[k(-\mathrm{i}W_2 + \sqrt{1+W_2^2})z] + B_4\exp[-k(\mathrm{i}W_2 + \sqrt{1+W_2^2})z], \quad (33)$$

The coefficients $\{A_1, \ldots, A_4\}$ and $\{B_1, \ldots, B_4\}$ multiplying the four linearly independent solutions are determined from the boundary conditions at $z = 1$ and the interface conditions (23)–(26) at $z = 0$, and conditions (27)–(30) at $z = \beta$. The most general solution to the fourth-order differential equation governing the dynamics of the solid layer, (22), has four linearly independent solutions and four coefficients multiplying these solutions. Two of the coefficients can be expressed in terms of the other two after using the zero displacement conditions ($\tilde{u}_z = 0, \tilde{u}_x = 0$) at $z = -H$, and we obtain:

$$\tilde{u}_z = C_1\{\exp[kz] - [1+2k(z+H)]\exp[-2Hk - kz]\} + C_2\{kz\exp[kz] + [k(2Hk(z+H) - z)] \times \exp[-2Hk - kz]\}. \quad (34)$$

The solutions for the fluid velocity in the two fluids Eqs. (32) and (33) and pressure fields and the solid layer displacement (34) and pressure fields are then inserted into the conditions at the interface, (23)–(31), and the boundary conditions at $z = 1$, viz. $\tilde{v}_z^{(1)} = 0, \tilde{v}_x^{(1)} = 0$, to obtain the characteristic matrix of the form:

$$\mathbf{M}\cdot\mathbf{C}^{\mathrm{T}} = 0, \quad (35)$$

where $\mathbf{C}$ is the vector of coefficients

$$\mathbf{C} = [A_1, A_2, A_3, A_4, B_1, B_2, B_3, B_4, C_1, C_2], \quad (36)$$

and $\mathbf{M}$ is a 10×10 matrix in which the ten rows are obtained from the four conditions at the fluid–fluid interface, four conditions at the fluid–solid interface and two conditions at the top rigid wall $z = 1$.

The characteristic equation is obtained by setting the determinant of the characteristic matrix $\mathbf{M}$ to zero. For fixed (nonzero) values of W_1, W_2, β, H, η_{r}, Γ, Σ and k, the characteristic equation turns out to be a polynomial of fifteenth degree for the complex wavespeed c. The solution to the problem was coded in the symbolic package Mathematica, and *all* the roots of the characteristic equation are obtained. Out of these fifteen solutions to c, there are two interfacial modes corresponding to the fluid–fluid interface and fluid–solid interface. All the other modes are verified to be stable, and we eschew the discussion of these modes hereafter. In addition to these discrete modes, it is well known [1] that there exists also a continuous spectrum of modes in the two fluids which are obtained by setting the coefficient of the term with the highest derivative in Eq. (18) to zero. Since the continuous spectrum in the two UCM fluids is always stable, attention is henceforth restricted only to the two interfacial modes at the two-fluid and fluid–solid interfaces, which are the ones that become unstable. Our general formulation for the characteristic equation for two-layer viscoelastic Couette flow past a deformable solid layer yields as special cases the configurations of two-layer flow of UCM fluids in rigid channels [1,2], and the flow of a single UCM fluid past a deformable solid layer [15].

3. Results

3.1. Two-layer viscoelastic Couette flow in rigid channels

It is first instructive to briefly recapitulate the results for the stability of two-layer Couette flow of UCM fluids in a rigid-walled channel, and this has been the subject of the earlier studies of Renardy [1] and Chen [2]. Renardy [1] used a short wave asymptotic analysis to show that mere elasticity stratification is sufficient to destabilize the two fluid interface in the creeping flow limit. Chen [2] analyzed the complementary asymptotic limit of long waves, and again showed that the two fluid interface is unstable due to elasticity stratification between the two fluids. Chen further showed that the long wave instability is present only when the more elastic fluid is of smaller thickness. While these authors probed the limiting cases of long and short waves, the most unstable mode could have finite wavelengths. From the formulation given in the previous section, we recover the rigid wall case by setting $\Gamma = 0$, and obtain the full dispersion relation, i.e., c_{r} and c_{i} versus k for all k. An example of this dispersion relation is shown in Fig. 2, for the case $W_1 > W_2$, while $\beta = 0.49$, 0.5 and 0.51. This figure clearly shows that when the thickness of the more elastic fluid is greater than or equal to the thickness of less elastic fluid, the interfacial mode is stable in the longwave limit ($k \to 0$), while when the thickness of the more elastic fluid is smaller, the interfacial mode becomes unstable in the longwave limit. However, as shown in Fig. 2(b), regardless of the thickness of the more elastic fluid, perturbations with finite wavelength do become unstable, and the maximum growth rate for all the three thickness values are very nearly equal. The fastest growing waves have $k \sim O(1)$ independent of the fluid thickness. The interfacial instability persists for higher wavenumbers regardless of the thickness of the more elastic fluid, and waves with $k \gg 1$ remain unstable since the interfacial tension in the fluid–fluid interface $\Sigma = 0$.

We have verified from our results that $c_{\mathrm{i}} \propto k$ for $k \ll 1$, while $c_{\mathrm{i}} \propto 1/k$ for $k \gg 1$. When expressed in terms of the real part of the growth rate $s_{\mathrm{r}} = kc_{\mathrm{i}}$, these results become $s_{\mathrm{r}} \propto k^2$ for $k \ll 1$, and $s_{\mathrm{r}} =$ constant for $k \gg 1$. These scalings are in agreement with the earlier results of Chen [2] and Renardy [1], thereby showing that the results

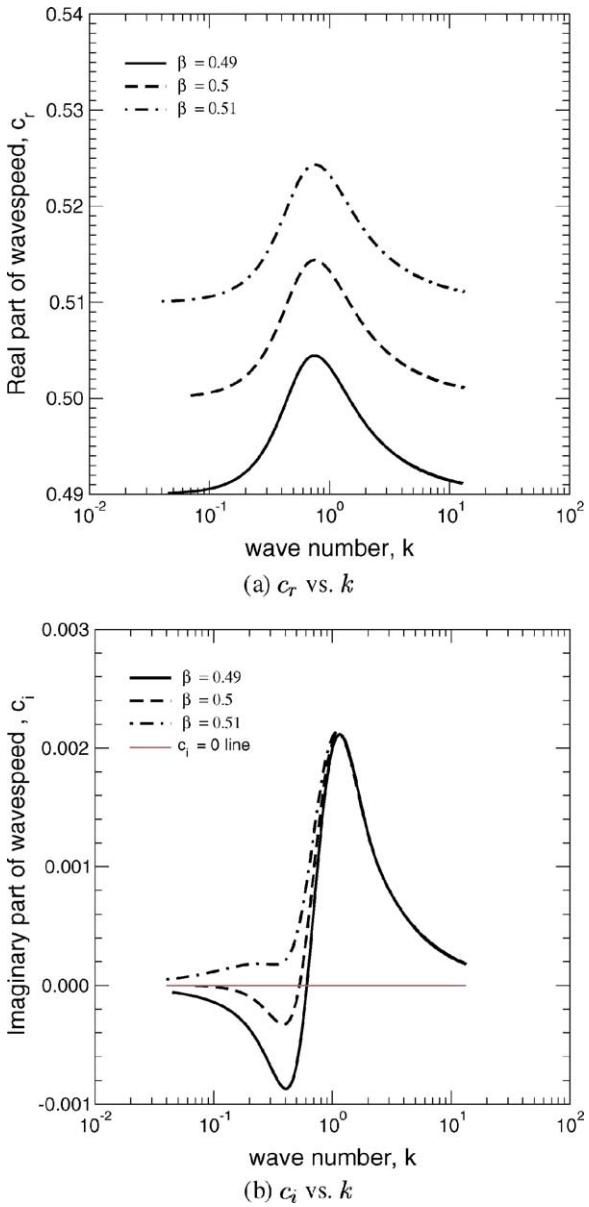

Fig. 2. Mode 1 instability in rigid channels: variation of the real and imaginary parts of the wavespeed c with the wavenumber k for two-layer UCM Couette flow in rigid channels ($\Gamma = 0$) for different fluid thickness ratio β: $W_1 = 6$, $W_2 = 5$, and interfacial tension $\Sigma = 0$.

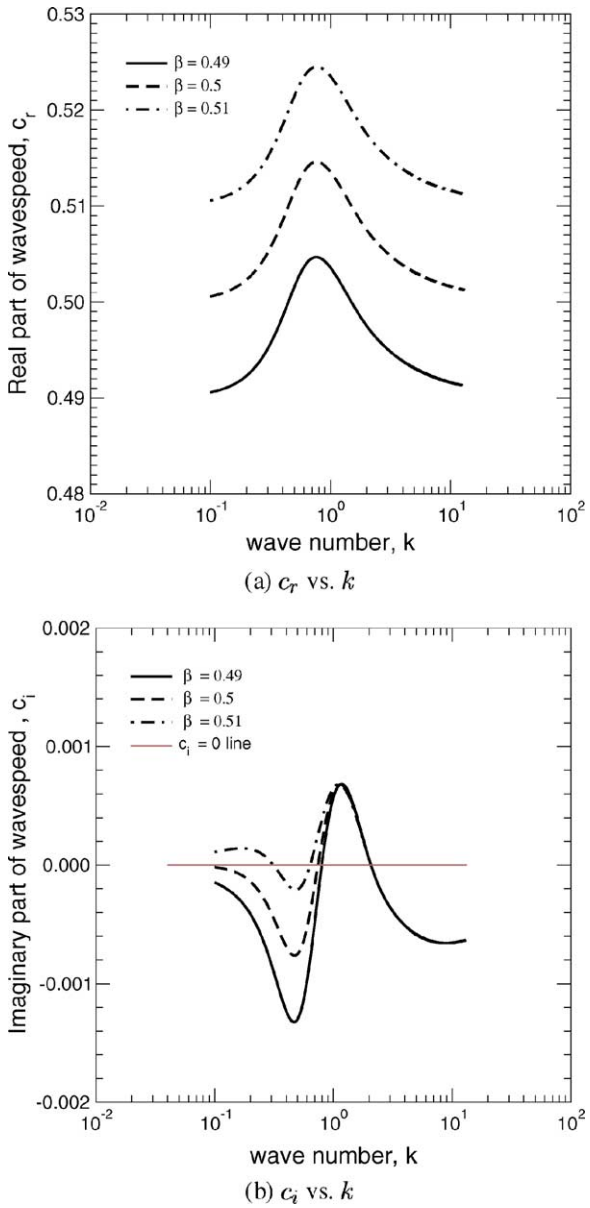

Fig. 3. Mode 1 instability in rigid channels: variation of the real and imaginary parts of the wavespeed c with the wavenumber k for two-layer UCM Couette flow in rigid channels ($\Gamma = 0$) for different fluid thickness ratio β: $W_1 = 6$, $W_2 = 5$, and interfacial tension $\Sigma = 1$.

of Chen and Renardy are asymptotic representations of the *same* unstable interfacial mode respectively at $k \ll 1$ and $k \gg 1$. The most unstable waves, however, have $k \sim O(1)$. We have also compared the wavespeed obtained from our formulation (with $\Gamma = 0$ for rigid channels) with the earlier low k asymptotic results of Chen [2], and this shows that our results are in exact agreement with the asymptotic expression given in [2] for $k \ll 1$, while for $k > 1$ the low k asymptotic analysis is not accurate. Fig. 3 shows that nonzero interfacial tension Σ in the two-fluid interface removes the shortwave instability, while the most unstable modes still have $k \sim O(1)$. The real part of the wavespeed c_r is unaffected by nonzero Σ.

Thus, the two-layer Couette flow of UCM fluids in rigid-walled channels becomes unstable whenever the relaxation times (or the Weissenberg number) of the two fluids are different. We refer this interfacial mode between the two UCM fluids as '*mode 1*'. Before turning to the effect of solid layer deformability on mode 1, it is useful to briefly recall the results of Shankar and Kumar [15] who studied the stability of the interface between a *single* UCM fluid (undergoing plane Couette flow) and a deformable solid layer. This interface becomes unstable when the parameter $\Gamma = V\eta/(GR)$ exceeds a critical value for a fixed Weissenberg number $W = \tau V/R$. The variation of c_i with k for different values of Γ is shown in Fig. 4, and this shows that

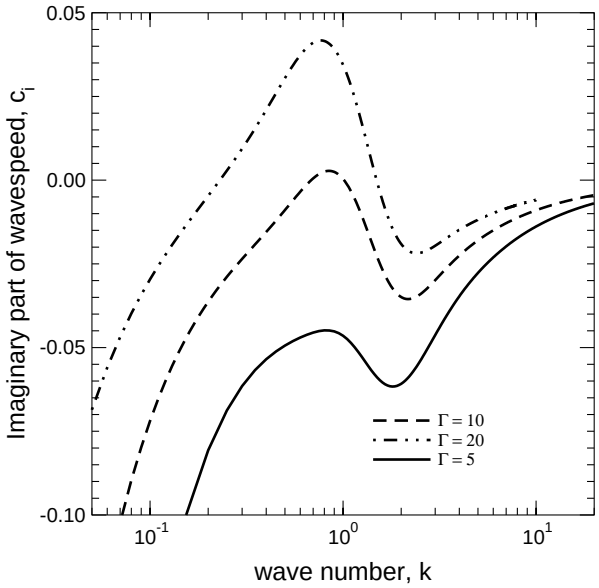

Fig. 4. Mode 2 in a single fluid for Couette flow of a UCM fluid past a deformable solid layer: variation of c_i with k for $W_1 = W_2 = 1$, $H = 1$, $\eta_r = 0$, and various values of Γ. Increase of Γ destabilizes mode 2 (Shankar and Kumar [15]).

the unstable perturbations have finite wave lengths, while both $k \ll 1$ and $k \gg 1$ perturbations are stable. We refer this interfacial mode between the UCM fluid and the solid layer as '*mode 2*'.

3.2. More elastic fluid in between less elastic fluid and solid layer

We first discuss the three-layer configuration where the more elastic fluid (fluid 2) is in between the less elastic fluid (fluid 1) and the solid layer. In this case, if $\beta < 1/2$, there is a longwave mode 1 instability in rigid channels. The effect of increasing Γ on mode 1 and mode 2 for $\beta = 0.4$ is shown in Fig. 5a and b. Fig. 5(a) shows that increasing Γ from zero does not alter the behaviour at $k \to 0$ for mode 1, but as k increases, c_i starts deviating from its rigid-channel value. For $k \sim O(1)$, c_i increases substantially due to increase in Γ and the growth rate of the most unstable mode also increases with Γ. For $k \gg 1$, c_i approaches the behaviour corresponding to two-layer flow in a rigid channel, as the short wave mode 1 instability between the two UCM fluids is expected to be insensitive to the presence of the deformable solid layer. However, when Γ is increased above a certain value, mode 1 is completely stabilized, except for waves with $k \to 0$. In Fig. 5(a), for $\Gamma = 10$, as $k \ll 1$, c_i coincides with its rigid channel value. As k increases, c_i becomes negative and remains so even for $k \gg 1$, and it does not show the high-k behaviour characteristic of mode 1. Note here that for $\Gamma = 0$, i.e., in rigid-walled channels, there is only mode 1 instability.

The corresponding behavior of c_i versus k for mode 2 as Γ is increased is shown in Fig. 5(b). Here, for $\Gamma = 5$ and 7, mode 2 remains stable for all k. However, for $\Gamma = 8$ and higher, mode 2 becomes unstable at finite k, and this instability persists even for large k. At large k, however, the c_i for mode 2 merges with the c_i obtained for two-layer flow in rigid channels. This shows that when Γ is greater than a critical value, as k is increased, mode 1 and mode 2 get 'switched' and it is mode 2 that shows the appropriate high k instability, and mode 1 remains stable except for very low k. At the critical value of Γ, both mode 1 and mode 2 have the same c_r and c_i at a particular value of wavenumber k. An analogous switching of the real part of wavespeed c_r for modes 1 and 2 is shown in Fig. 5(c) and (d). In order to illustrate the switching of mode 1 and mode 2 in a better way, we show c_i versus k for both mode 1 and mode 2 in Fig. 6(a) and c_r versus k in Fig. 6(b). This clearly shows that for Γ smaller than a critical value, mode 1 has $c_i \to 0$ for $k \to 0$, and $c_i \to 0$ for $k \gg 1$. However, for Γ greater than the critical value, mode 1 has $c_i \to 0$ for $k \ll 1$, but as k is increased it becomes completely stable. For Γ greater than the critical value, mode 2 is stable for $k \to 0$, but it becomes unstable at finite k, and remains unstable at all higher values of k. At a fixed value of k, however, if the modes 1 and 2 are tracked as a function of Γ, the variation of c_r and c_i is continuous.

We further note that when the two modes (1 and 2) get switched at intermediate k as Γ is increased, the labels mode 1 and mode 2 are clearly arbitrary. We use the nomenclature based on the behaviour of the two interfacial modes as $k \to 0$, and we designate the mode with $c_i \to 0^+$ for $\beta > 1/2$ ($c_i \to 0^-$ for $\beta \leq 1/2$) and $c_r \to \beta$ as mode 1 (which is the appropriate low k behaviour of the interfacial mode for two-layer UCM flow in rigid channels). The other interfacial mode (between fluid 2 and the solid layer) is heavily damped as $k \to 0$, and is identified as mode 2. Regardless of the nomenclature, the results clearly show that the low-k and high-k behaviour of the two modes gets interchanged as Γ is increased beyond a certain value. Our results show that the exchange of the two modes at finite k takes place when Γ is fixed, but H (the nondimensional solid layer thickness) is increased, thereby making the solid layer more deformable. Fig. 7 demonstrates the exchange of the two modes by enlarging the parameter space where the exchange takes place, when H is increased from 8.1 to 8.2. This plot in magnified parameter space clearly shows that at a certain critical H and k, the real and imaginary part of the wavespeeds of modes 1 and 2 coincide. When H is less than this critical value, mode 1 has the behaviour that as $k \to 0$ $c_i \to 0$, and for $k \gg 1$, $c_i \to 0$. Whereas, for H greater than this critical value, $c_i \to 0$ for $k \ll 1$, but mode 1 is stabilized for all higher k. On the other hand mode 2 becomes unstable at finite k, and all higher k waves are unstable, with c_i for mode 2 coinciding with that of mode 1 for two-layer flow in rigid channels for $k \gg 1$.

The foregoing discussion thus illustrates that the solid layer deformability has a dramatic effect on the two interfacial modes: when the wall is sufficiently deformable, mode 1

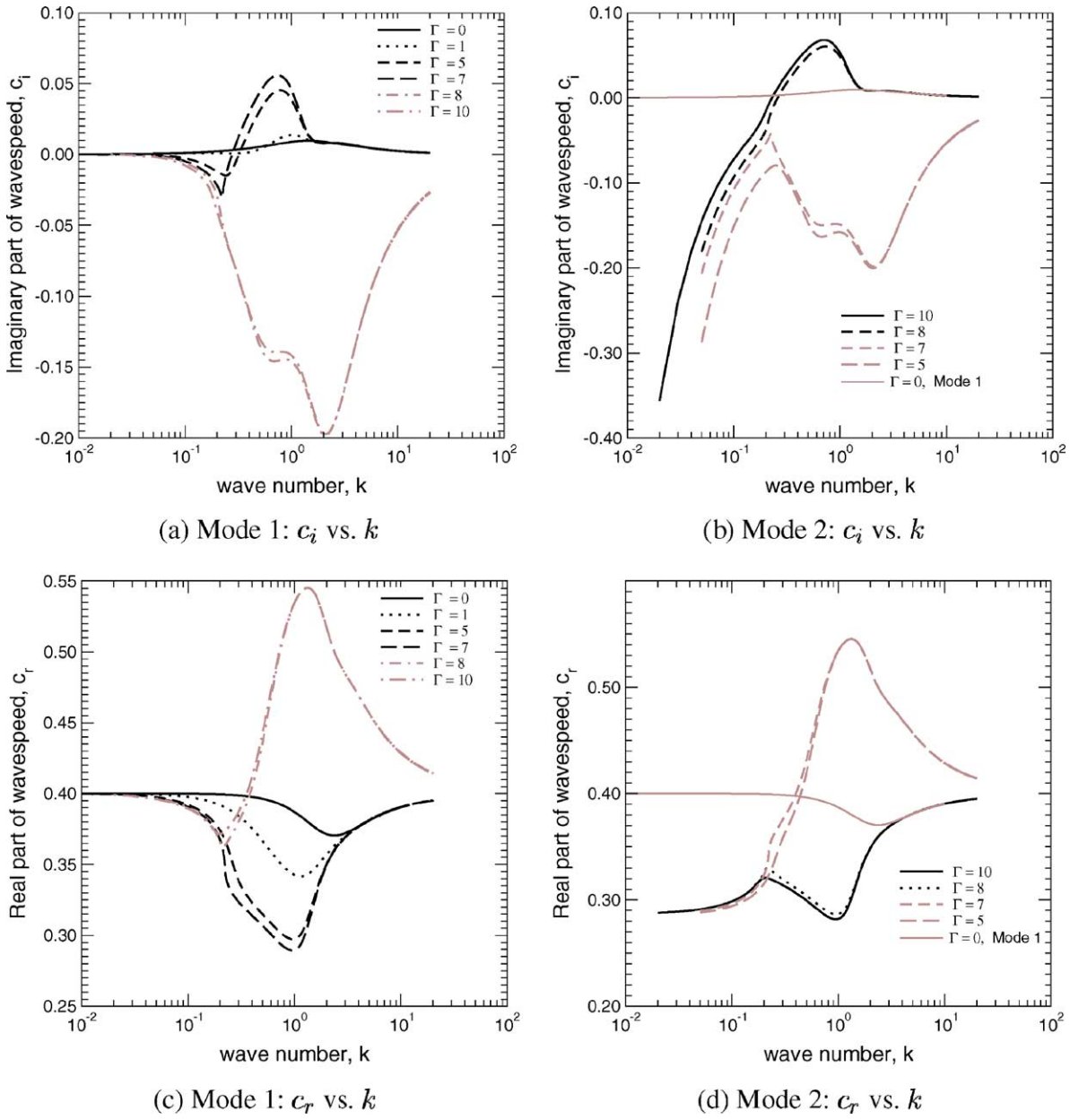

(a) Mode 1: c_i vs. k

(b) Mode 2: c_i vs. k

(c) Mode 1: c_r vs. k

(d) Mode 2: c_r vs. k

Fig. 5. Effect of solid layer deformability on mode 1 and mode 2: illustration of 'mode switching' at intermediate k : $W_1 = 1, W_2 = 2, \beta = 0.4$, $\eta_r = 0, H = 1$.

is stabilized for all k except $k \to 0$, while mode 2 is unstable for finite k and approaches the behaviour of two-layer UCM flow in rigid channels for large k. When Γ is lesser than a threshold value, mode 1 has the same asymptotic behaviour at $k \ll 1$ and $k \gg 1$ as in rigid channels, but at finite k, the growth rate (proportional to c_i) is greatly enhanced due to solid layer deformability. This is illustrated for two parameter sets in Fig. 8. For the parameters shown in this figure, mode 2 remains stable. Thus, it is possible to enhance the growth rate of the interfacial mode between the two UCM fluids by making the solid layer more deformable, but at the same time not excite the mode 2 instability between fluid 2 and the solid layer. We have also verified that when $\beta > 0.5$, and for W_1 and W_2 such that mode 1 is completely stable at all k in rigid channels, it is possible to excite only the mode 2 instability by increasing Γ.

The results provided in the preceding discussion are for purely elastic solid layers with $\eta_r = 0$. The effect of η_r on mode 1 (for fixed values of Γ, W_1 and W_2) was examined, and this indicates that nonzero viscosity in the solid layer has a stabilizing effect on mode 1. Fig. 9 shows the effect of elasticity stratification on mode 2 instability between the fluid 2 and the solid layer. Mode 1 is stable for the parameter set considered in this figure. Also plotted in this figure is the variation of c_i versus k for a single fluid flow past a deformable solid with $W_1 = W_2 = W$, for both $W = 1$ and

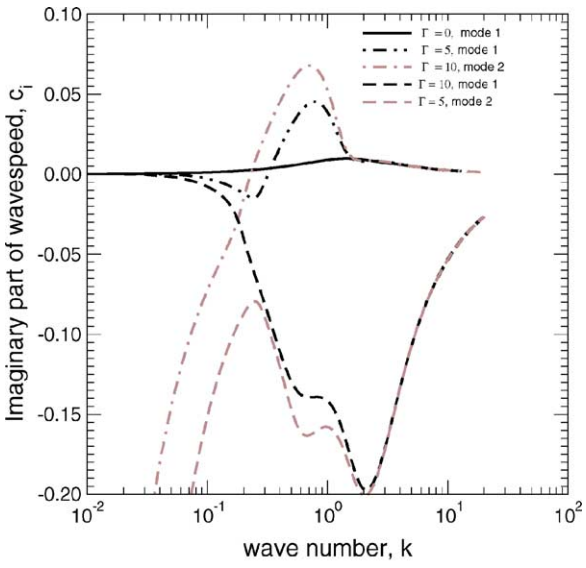

(a) c_i vs. k

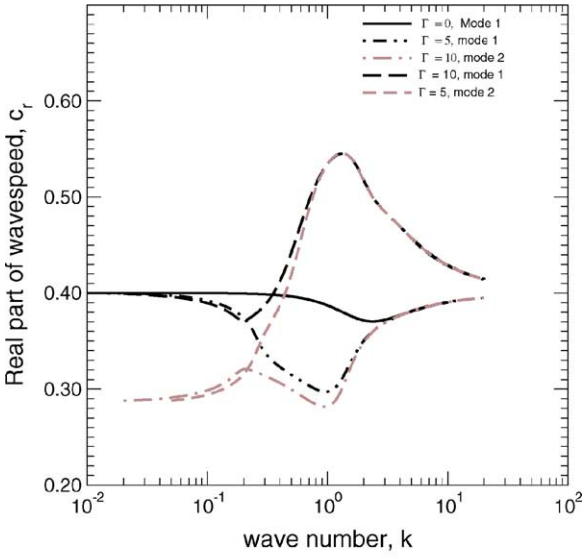

(b) c_r vs. k

Fig. 6. Effect of solid layer deformability on mode1 and mode 2: $W_1 = 1$, $W_2 = 2$, $\beta = 0.4$, $\eta_r = 0$, $H = 1$.

$W = 2$ for the sake of comparison. If there were no interactions between the fluid–fluid interface and the fluid–solid interface, one might expect that the c_i versus k for the case in which $W_1 = 1$ and $W_2 = 2$ would lie somewhere in between the two curves for the single fluids with $W = 1$ and $W = 2$. However, this figure shows that the maximum growth rate for the case with elasticity stratification is much *larger* than the case when there is a single fluid–solid interface. This clearly shows that the interfacial perturbations at the fluid–fluid and fluid–solid interface interact strongly.

The fact that mode 1 is stabilized (except for very long waves) for sufficiently large Γ, but mode 2 is unstable, raises the following question: Is it possible to stabilize mode 2 by changing the viscosity ratio η_r (ratio of solid to fluid viscosities)?. The motivation for this possibility comes from the earlier results of Shankar and Kumar [15], who showed that for the case of the interface between a single UCM fluid and a solid layer, η_r has a stabilizing effect on the mode 2 instability. This possibility is explored in Fig. 10, where we consider a configuration where $W_1 < W_2$ and $\beta < 1/2$, so that in a rigid channel the flow is unstable at all k in the absence of interfacial tension ($\Sigma = 0$). Fig. 10(a) shows that for $\eta_r = 0$ and $\Gamma = 10$, mode 1 is completely stable, except for $k \to 0$ and $k \gg 1$. Mode 2 is unstable for a finite range of $k \sim O(1)$. Fig. 10(b) shows the effect of increasing η_r to 1, and this shows that mode 2 is completely stabilized, and mode 1 is stable except for $k \ll 1$ and $k \gg 1$. However, the presence of a nonzero interfacial tension between the two fluid interface $\Sigma \neq 0$ stabilizes the interfacial mode 1 at high k. Fig. 11 shows the variation of c_i with k for modes 1 and 2, with $\Sigma = 0.1$ for two different parameter sets. This shows that for $\eta_r \neq 0$ and $\Sigma \neq 0$, mode 2 is completely stable for all k, while mode 1 is stable except for very long waves $k \to 0$. We have verified that the stabilizing effect of solid layer deformability on both modes 1 and 2 occurs for a variety of parameter sets, and these results demonstrate that the presence of the solid layer has a dramatic effect on the purely elastic interfacial instability between the two UCM fluids, when the more elastic fluid is in between the less elastic fluid and the solid layer. In Fig. 12, we demonstrate that by careful choice of Γ and η_r, it is possible to either enhance or suppress the mode 1 instability between the two UCM fluids, for fixed values of W_1, W_2 and β. The above results therefore open up the possibility that soft solid layer coatings can potentially be used to suppress or enhance the purely elastic interfacial instability between the two UCM fluids, by carefully tuning the shear modulus (or, equivalently, Γ) and the loss modulus (or, equivalently, η_r) of the viscoelastic solid, so that mode 2 instability between the solid and the fluid is not excited.

While the foregoing illustrations (using c_i versus k plots) of stabilization of mode 1 are for a selective parameter values of Γ, it is instructive to construct neutral stability curves (curves of $c_i = 0$), in the Γ–k plane for fixed values of W_1, W_2, η_r, H and β. Such plots will then allow us to select the parameter Γ so that both mode 1 and mode 2 are stable. Fig. 13(a) and (b) show the neutral stability curves for the cases with $\eta_r = 0$ and $\eta_r = 1$. Note that for the two-fluid configuration under consideration here, there is a mode 1 interfacial instability in rigid channels (i.e., $\Gamma = 0$ in our framework) for $W_1 < W_2 \neq 0$ and $\beta < 1/2$. Therefore, in these figures, the line $\Gamma = 0$ is completely unstable for all k in the absence of interfacial tension Σ. The neutral stability curves for both mode 1 and mode 2 are plotted: when Γ *increases* beyond the neutral curve for mode 1, there is a *transition from unstable waves to stable waves* of mode 1. Whereas, when Γ increases beyond the neutral curve for mode 2, there is a *transition from stable waves to unstable waves* of mode 2. These curves clearly show that solid

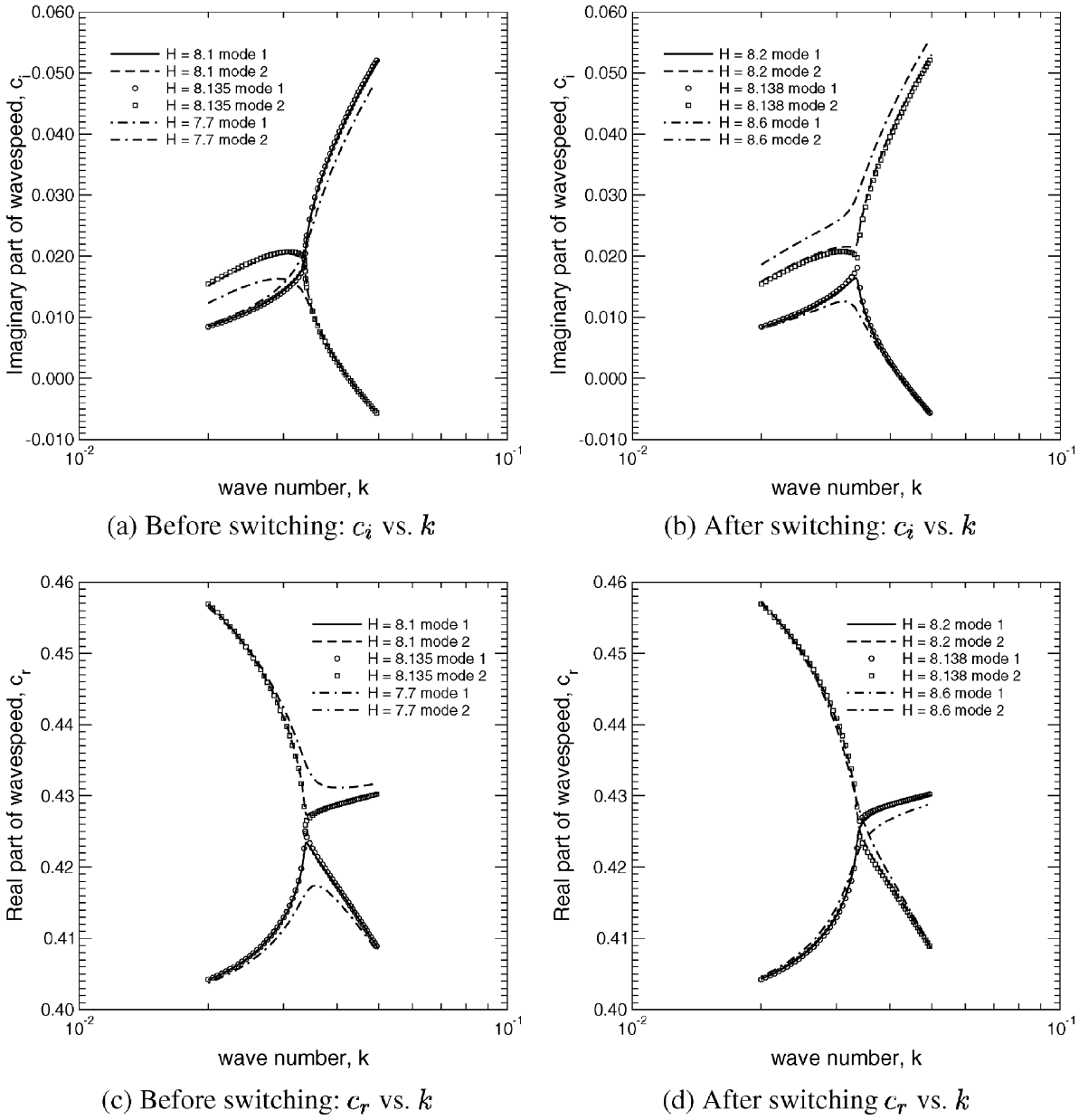

(a) Before switching: c_i vs. k

(b) After switching: c_i vs. k

(c) Before switching: c_r vs. k

(d) After switching c_r vs. k

Fig. 7. Demonstration of switching of mode 1 and mode 2 by zooming in the parameter space. When the data is plotted in symbols (squares and circles) only a few representative points are plotted for clarity. Data for $W_1 = 5$, $W_2 = 6$, $\eta_r = 0$, $\Gamma = 5$, $\beta = 0.4$.

layer deformability has a stabilizing effect on mode 1, but destabilizing effect on mode 2, and there is a sufficiently wide window of the parameter Γ in which both mode 1 and mode 2 are stable. For the mode 1 neutral curve, $\Gamma \sim 1/k$ for $k \ll 1$, meaning that the solid layer elasticity should decrease with a decrease in wavenumber in order to stabilize long waves of mode 1. In these figures, the interfacial tension $\Sigma = 0$, so mode 1 is unstable at very high wavenumbers regardless of Γ, since the high wavenumber mode 1 instability is localized at the fluid–fluid interface and is insensitive to the deformability of the solid layer. Fig. 13(b) shows the same parameter set as Fig. 13(a), except that η_r is increased to 0.6. The effect of nonzero η_r is to stabilize mode 2, i.e., to increase the critical value of Γ required to excite the mode 2 instability.

Fig. 14(a) and (b) shows the role of nonzero interfacial tension between the two fluids, Σ, on the neutral curves for two different values of η_r, with all the other parameters remaining the same as in Fig. 13(a) and (b). The presence of nonzero Σ stabilizes high k waves for the mode 1 instability, and so the unstable region in the Γ–k plane is now restricted to finite and low k region. Nonzero Σ between the two fluids clearly does not have any effect on the mode 2 neutral curve, which remains the same as in Fig. 13(b). Increasing η_r from 0.6 to 1 completely stabilizes mode 2 (see Fig. 14(b)), and thus it is possible to choose the nondimensional

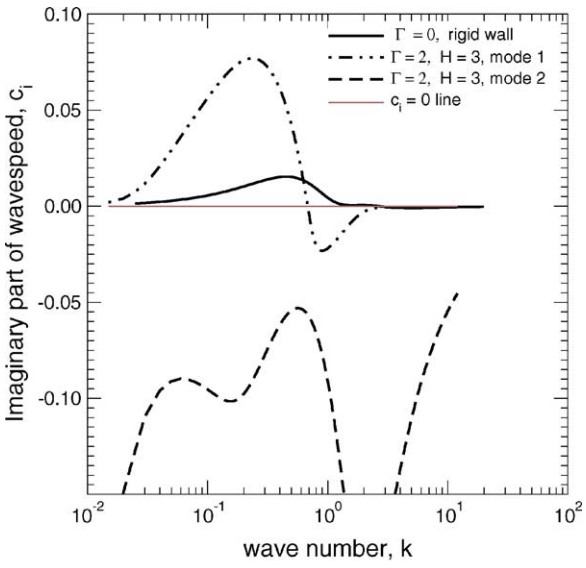

(a) $W_1 = 0, W_2 = 5, \beta = 0.4$

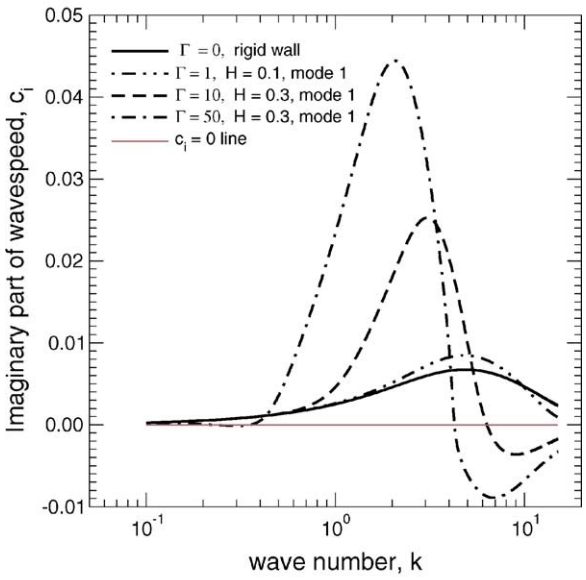

(b) $W_1 = 0.1, W_2 = 0.5, \beta = 0.1$

Fig. 8. Enhancement of mode 1 instability due to solid layer deformability when mode 2 is stable: $\Sigma = 0$, $\eta_r = 0$ in both cases.

elasticity parameter Γ as large as possible to completely stabilize the mode 1 instability. For realistic experimental geometries, the lowest value of wavenumber k that is allowed is inversely proportional to the system length, so by choosing sufficiently large Γ it should be possible to completely suppress mode 1 interfacial instability between the two fluids in finite experimental geometries. Fig. 15 shows the neutral curves for mode 1 and mode 2 for different parameter sets, and this further demonstrates that it should be possible to completely suppress mode 1 instability in finite experimental systems, by increasing the deformability of the wall (i.e., Γ). By modifying η_r of the solid layer, it is also possible to completely suppress the mode 2 interfacial instability.

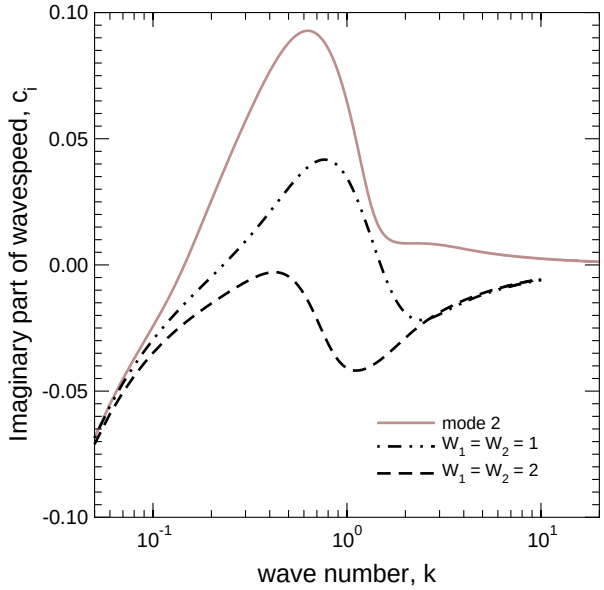

Fig. 9. Effect of elasticity stratification on mode 2 instability: $W_1 = 1$, $W_2 = 2$, $H = 1$, $\beta = 0.4$, $\Gamma = 20$, $\eta_r = 0$. Also shown are the results for mode 2 in a single UCM fluid with $W_1 = W_2 = 1$, and $W_1 = W_2 = 2$.

The discussion thus far was concerned with the case where the more elastic fluid of smaller thickness is present between the less elastic fluid of larger thickness and the solid layer. The configuration in which the more elastic fluid of larger thickness in between the less elastic fluid and the solid layer was also considered. In a rigid channel, such a configuration undergoes only finite wavenumber instability, and $k \to 0$ modes are stable, while modes with $k \gg 1$ are stabilized by the nonzero interfacial tension. The effect of solid layer deformability was found to be purely stabilizing on these finite k unstable waves of mode 1. We, therefore, do not provide any further discussion on this configuration.

3.3. Less elastic fluid in between more elastic fluid and solid layer

We now turn to the discussion of the configuration where the less elastic fluid is in between the more elastic fluid and the solid layer. We first discuss the case where the thickness of the less elastic fluid is larger than the more elastic fluid. Such a configuration is unstable to waves with any k in a rigid channel (when the interfacial tension $\Sigma = 0$). When the more elastic fluid is present in between the less elastic fluid and the solid layer, we demonstrated in the previous Section 3.2 that mode 1 can be completely stabilized. Fig. 16(a) shows the effect of solid layer deformability on the variation of c_i with k for the case when the less elastic fluid 2 (with $W_2 = 0.1$) of larger thickness $\beta = 0.6$ is in between the more elastic fluid 1 (with $W_1 = 0.5$) of smaller thickness $(1-\beta) = 0.4$ and the solid layer. Also plotted in these figures are the c_i versus k plots for the case considered in the previous section in which only the two fluid layers are flipped: the more elastic fluid 2 (with $W_2 = 0.5$) of smaller thickness

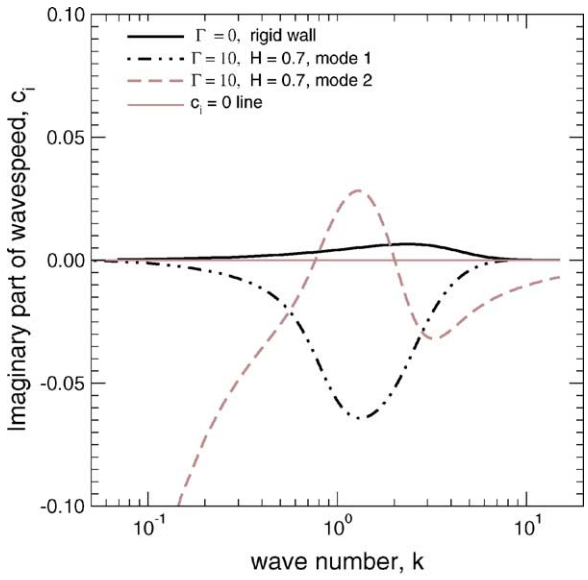

(a) $\eta_r = 0$

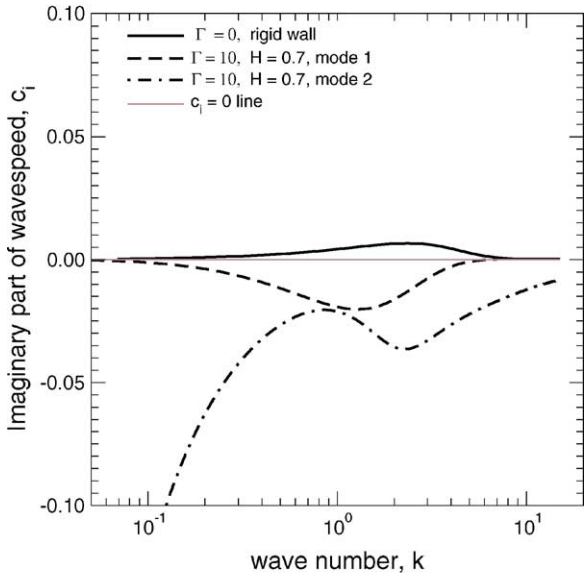

(b) $\eta_r = 1$

Fig. 10. Suppression of mode 1 and mode 2 instabilities due to solid layer deformability: effect of η_r for $W_1 = 0.1$, $W_2 = 0.5$, $\beta = 0.4$, $\Sigma = 0$.

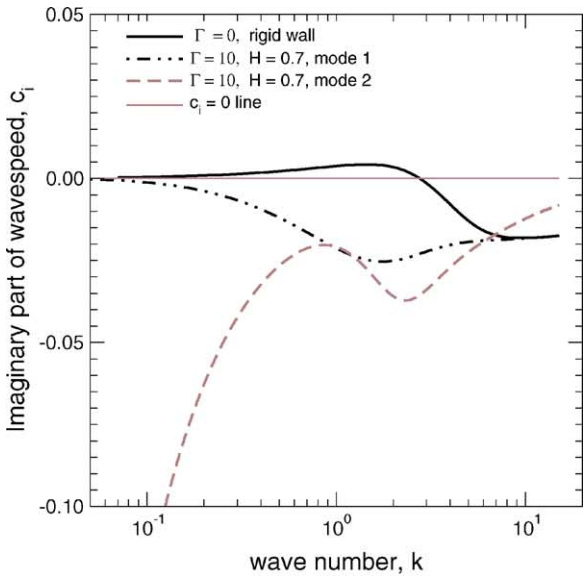

(a) $\Gamma = 10, H = 0.7$

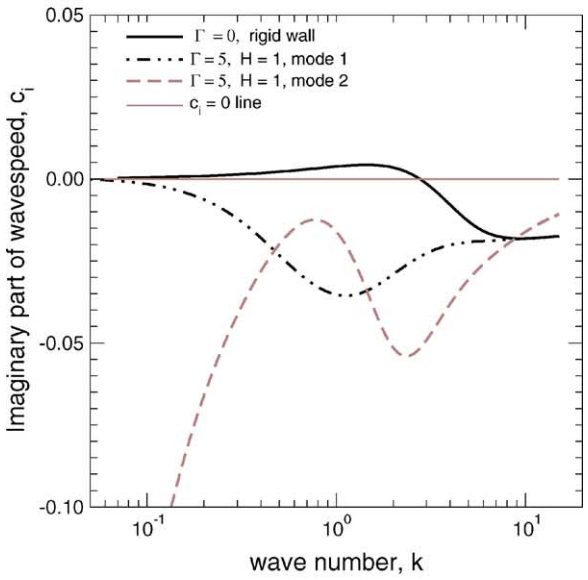

(b) $\Gamma = 5, H = 1$

Fig. 11. Suppression of mode 1 and mode 2 instabilities with nonzero interfacial tension between the two UCM fluids: demonstration of stabilization for two different set of solid layer parameters. $\Sigma = 0.1$, $\eta_r = 1$, $\beta = 0.4$, $W_1 = 0.1$, $W_2 = 0.5$.

$\beta = 0.4$ is in between the less elastic fluid 1 (with $W_1 = 0.1$) of larger thickness $(1 - \beta) = 0.6$. This figure shows that by merely interchanging the two fluid layers, the effect of solid layer deformability on mode 1 completely reverses: from being stabilizing for the configuration considered in the previous section, it becomes completely destabilizing for the configuration considered in this section. However, the effect of interchanging the fluid layers has only marginal effect on mode 2. Fig. 16(b) demonstrates this same effect for a different parameter set for the configuration where the less elastic fluid 2 of larger thickness is in between the more elastic fluid 1 and the solid layer.

We next turn to the discussion of the configuration where the less elastic fluid 2 of *smaller* thickness is in between the more elastic fluid 1 of *larger* thickness and the solid layer. In a rigid channel (without the solid layer), such a configuration is stable to waves with $k \to 0$, while only finite and short waves become unstable due to elasticity stratification. Fig. 17 shows the effect of solid layer deformability on the variation of c_i versus k for a variety of parameter sets. This figure shows that in this configuration, solid layer deformability has a completely destabilizing effect on mode 1, and

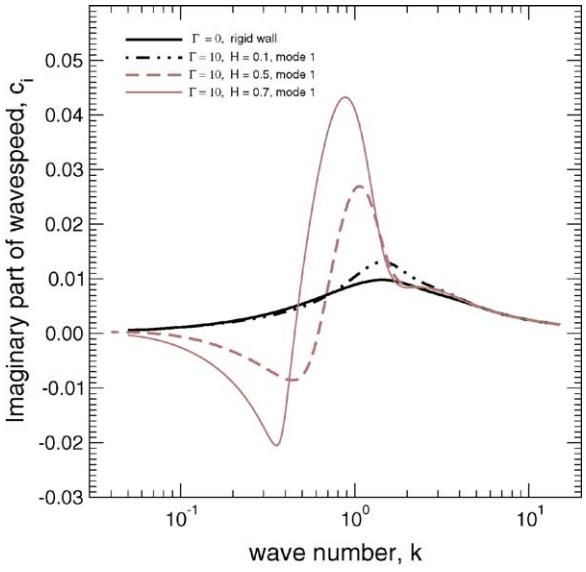

(a) $\Gamma = 10, \eta_r = 0, \Sigma = 0$

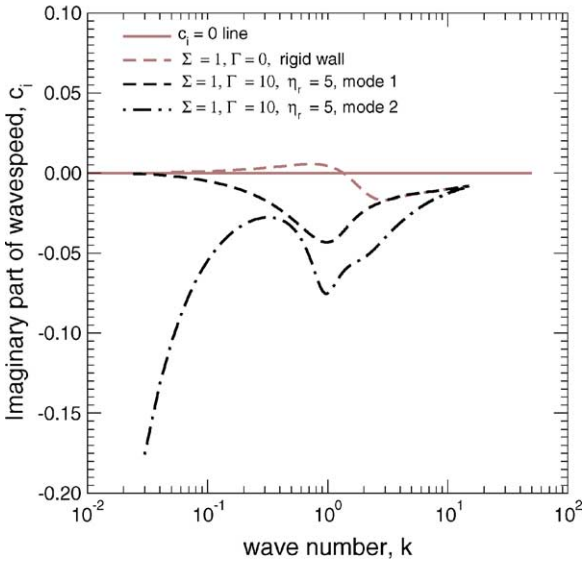

(b) $\Gamma = 10, H = 1, \eta_r = 5, \Sigma = 1$

Fig. 12. Enhancement and suppression of mode 1 instability by tuning the parameters characterizing the deformable solid layer: $W_1 = 1$, $W_2 = 2$, $\beta = 0.4$.

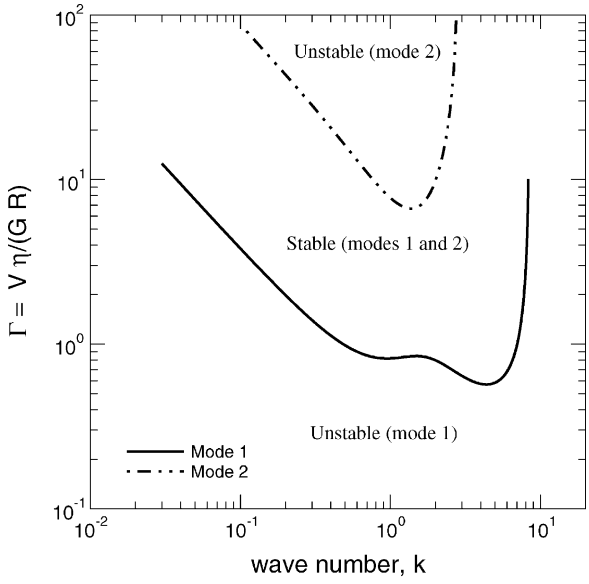

(a) $\eta_r = 0$

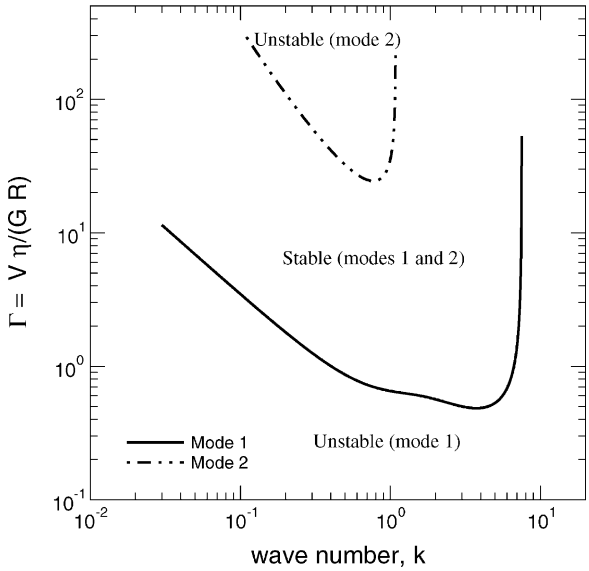

(b) $\eta_r = 0.6$

Fig. 13. Neutral stability curves for mode 1 and mode 2 instabilities for fixed W_1 and W_2 in the Γ–k plane: $W_1 = 0.1$, $W_2 = 0.5$, $\beta = 0.4$, $\Sigma = 0$, $H = 0.7$. Illustration of stabilization of mode 1 due to solid layer deformability (finite Γ), for the case where the interfacial tension Σ between the two UCM fluids is zero.

it destabilizes even waves with small k. At large k, there is an instability even in rigid channels in the absence of interfacial tension, and solid layer deformability does not affect those large k waves. Also shown in this figure, for the sake of comparison, are the results for the configuration in which only the two fluid layers are flipped (discussed in the previous section), where the more elastic fluid of larger thickness is in between the less elastic fluid of smaller thickness and the solid layer. In that configuration, wall deformability was shown to have a purely stabilizing effect. However, by merely interchanging the two fluid layers, the effect of solid layer deformability changes from being completely stabilizing to completely destabilizing. However, mode 2 is not very significantly affected due to the interchange of the two fluid layers. This trend continues even to the case when the two fluids have *equal* thicknesses $\beta = 1 - \beta = 0.5$. In this case, when the less elastic fluid is in between the more elastic fluid and the solid layer, mode 1 is unstable due to solid layer deformability. The configuration where the more elastic fluid is in between the less elastic fluid and the solid layer, on the other hand, is stabilized by solid layer deformability, while such a configuration is stable (except for large k) in

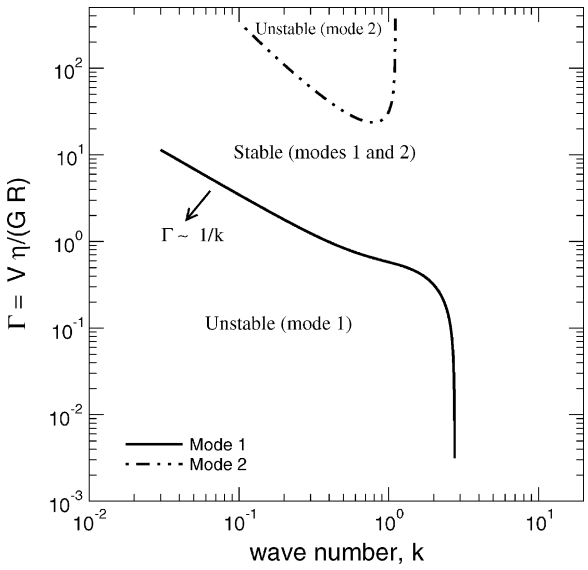

(a) $\eta_r = 0.6$

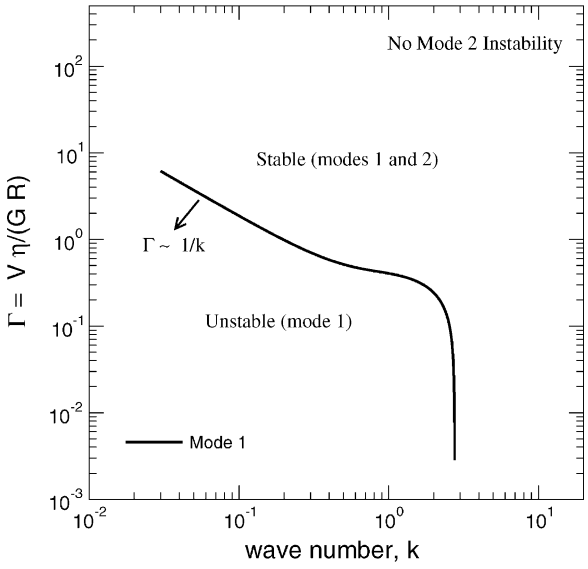

(b) $\eta_r = 1$

Fig. 14. Neutral stability curves for mode 1 and mode 2 instabilities for fixed W_1 and W_2 in the Γ–k plane: $W_1 = 0.1$, $W_2 = 0.5$, $\beta = 0.4$, $\Sigma = 0.1$, $H = 0.7$. Stabilization of mode 1 due to solid layer deformability (finite Γ) and mode 2 due to increase in η_r, for the case where the interfacial tension Σ between the two UCM fluids is nonzero.

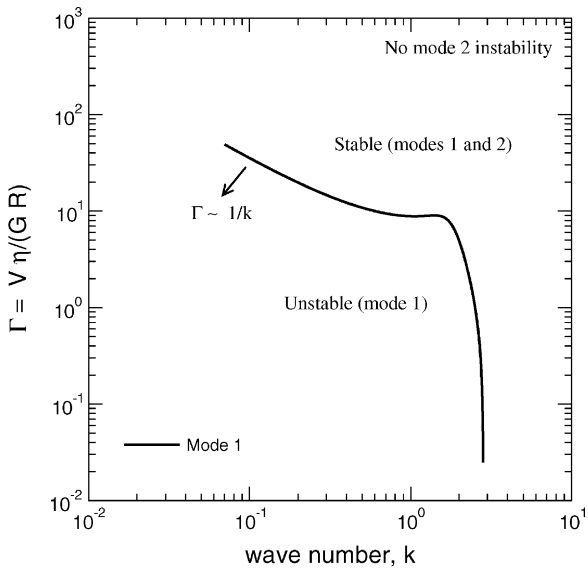

(a) $W_1 = 0.5, W_2 = 1, \Sigma = 0.1, \eta_r = 0, H = 0.2$

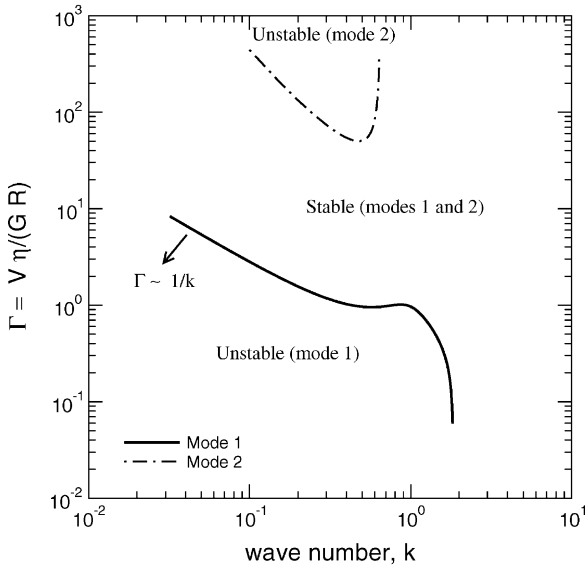

(b) $W_1 = 1, W_2 = 2, \Sigma = 0.5, \eta_r = 1, H = 0.8$

Fig. 15. Neutral stability curves for mode 1 and mode 2 instabilities for fixed W_1 and W_2 in the Γ–k plane: $\beta = 0.4$. Illustration of stabilization of mode 1 due to solid layer deformability.

rigid channels. For this case where the two fluids have equal thickness, mode 2 is found to be altered only marginally due to the interchanging of the two fluid layers.

Fig. 18 shows the neutral curves in the Γ–k plane for a few representative parameter sets for the configuration discussed above. In these figures, when Γ increases beyond the neutral curve for mode 1, there is a transition from stable to unstable region for mode 1, while mode 2 remains stable. Mode 2 becomes unstable at a significantly higher value of Γ, when Γ increases beyond the mode 2 neutral curve. These plots point to the possibility of using soft solid layer coatings to manipulate purely elastic interfacial instability in two-layer viscoelastic flows. By merely interchanging the fluid layers, it is possible to change the stability characteristics dramatically: from mode 1 being completely stable to being unstable. Note that in the absence of interfacial tension, Σ, waves with $k \gg 1$ are unstable for mode 1. Fig. 19 shows the role of nonzero interfacial tension, Σ, on the neutral curves, and this expectedly stabilizes short wave perturbations, thus making only a finite band of waves unstable upon increase of Γ. Also, the nondimensional parameter Γ required to excite the mode 1 instability scales as $\Gamma \sim 1/k$ for $k \ll 1$, meaning that the solid layer elasticity should de-

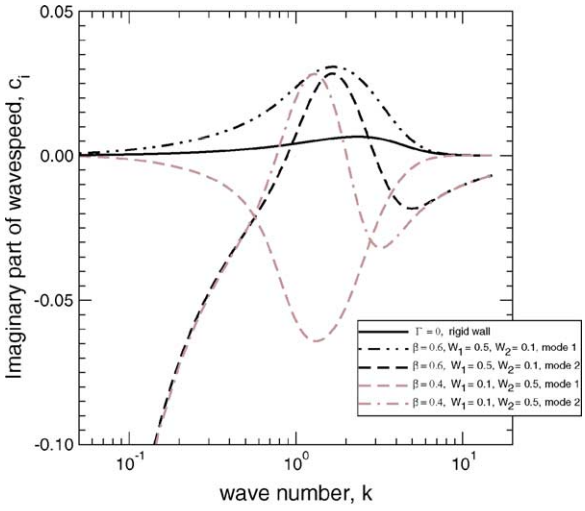

(a) $\Gamma = 10, \eta_r = 0, H = 0.7$

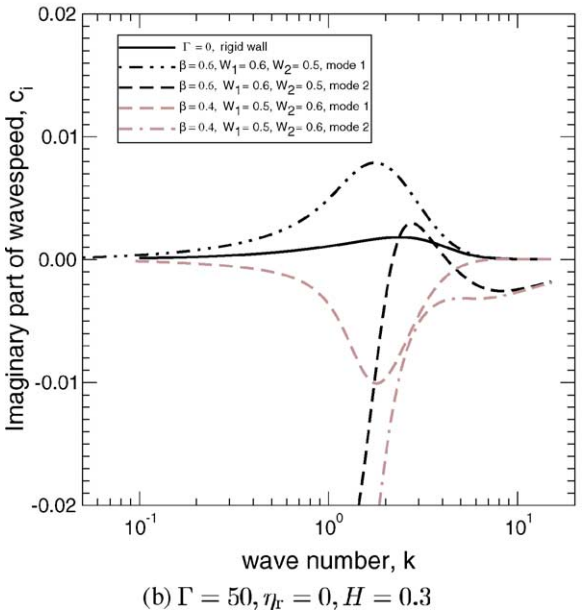

(b) $\Gamma = 50, \eta_r = 0, H = 0.3$

Fig. 16. Destabilization of mode 1 when the lesser elastic fluid of larger thickness is in between the more elastic fluid and the solid layer, for the configuration when mode 1 instability is already present in rigid walls.

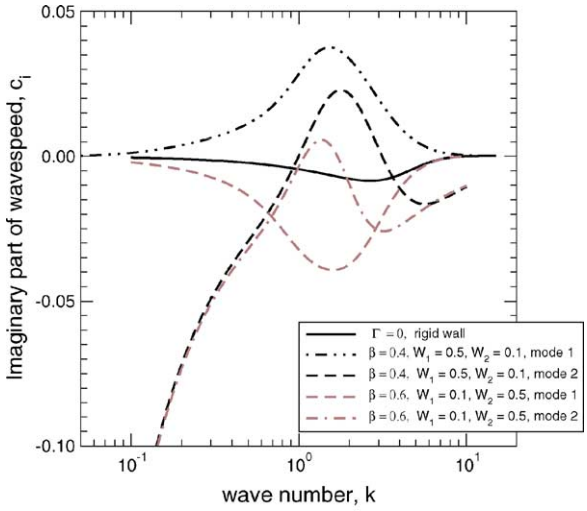

(a) $\Gamma = 10, \eta_r = 0, H = 0.7$

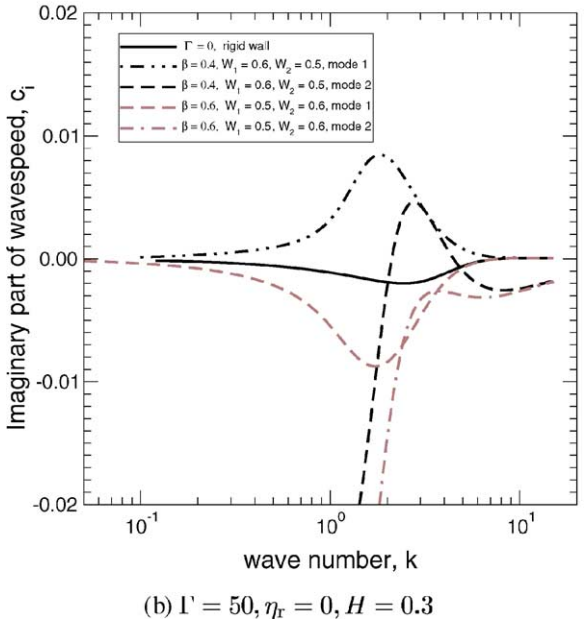

(b) $\Gamma = 50, \eta_r = 0, H = 0.3$

Fig. 17. Destabilization of mode 1 due to solid layer deformability *when it is stable in rigid channels*: when the less elastic fluid (of smaller thickness compared to the more elastic fluid) is in between the more elastic fluid and the solid layer.

crease as the inverse wavelength of perturbations for very long waves in order to render these (mode 1) long waves unstable.

Before closing this section, it is useful to compare and contrast the results obtained for the present three-layer configuration of two UCM fluids and a solid layer with that of Ganpule and Khomami [6] who considered (among various other configurations) the three-layer configuration of *three UCM fluids* without viscosity stratification. They considered the Weissenberg numbers of the three UCM fluids to be different, but the thickness of the top (fluid 1) and bottom (fluid 3) layers are equal, while the thickness of the middle (fluid 2) layer was varied relative to the top/bottom layer thickness. Thus, that configuration is identical to the present system except that we have a solid in the bottom layer instead of the UCM fluid. They identified two modes of purely elastic instability, one associated with each interface. When $W_1 < W_2 < W_3$ (see Figs. 17 and 18), and for arbitrary ratios of the thickness of fluid 2 with the thickness of the top and bottom layers, their results show that the interfacial mode corresponding to the top layer is stable to longwave disturbances. This is because, with respect to the top interface, the flow configuration is that of a thin layer of less elastic fluid, which is stable (as predicted by the longwave analysis of Chen [2]). However, the interfacial mode corresponding to the bottom layer is unstable because with

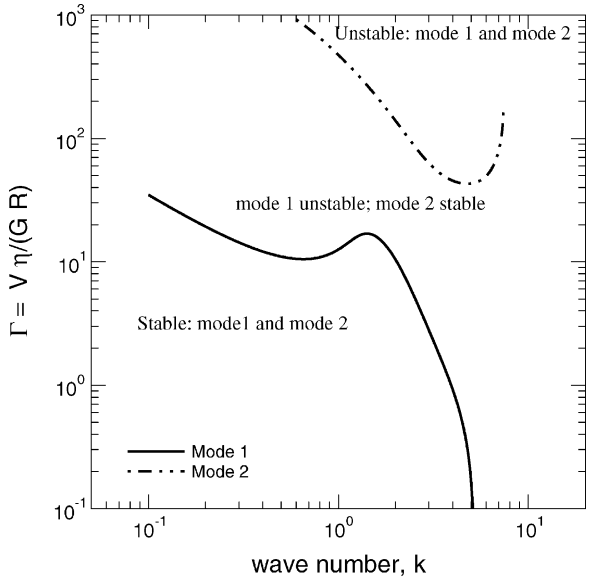

(a) $W_1 = 1, W_2 = 0.5, H = 0.2$

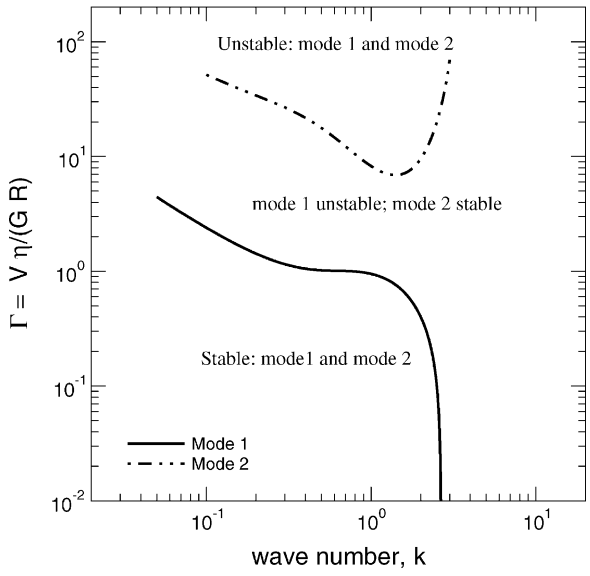

(b) $W_1 = 2, W_2 = 1, H = 0.2$

Fig. 18. Neutral stability curves for mode 1 and mode 2 instabilities for fixed W_1 and W_2 in the Γ–k plane: $\beta = 0.4$, $\eta_r = 0$, $\Sigma = 0$. Illustration of destabilization of mode 1 due to finite solid layer deformability, when it is stable in rigid channels. Less elastic fluid of smaller thickness is in between the more elastic fluid and the solid layer.

respect to the bottom interface, the flow configuration is that of a thin layer of more elastic fluid, which is unstable. However, for the configuration analyzed in this paper, $W_1 \neq W_2$ and instead of the fluid 3 we have a solid layer, the interfacial mode between the two fluids is stable or unstable depending on the nondimensional elasticity of the solid layer, and the relative thickness of the two fluids and their Weissenberg numbers. When the thickness of fluid 2 is smaller, and its Weissenberg number $W_2 > W_1$, then if the wall is made sufficiently deformable, the purely elastic unstable

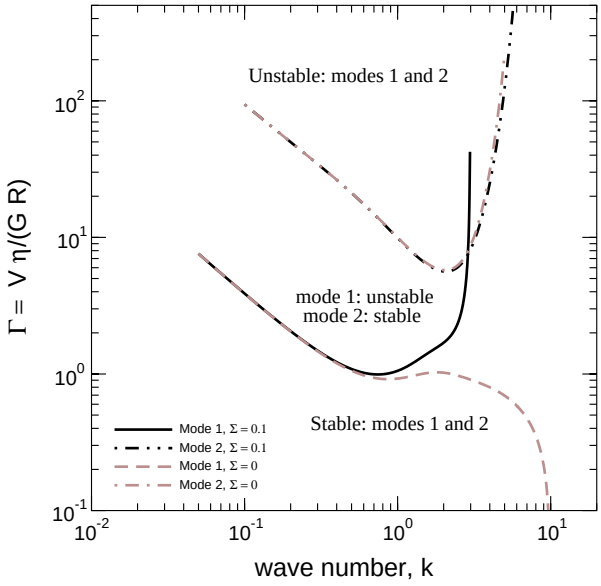

Fig. 19. Neutral stability curves for mode 1 and mode 2 instabilities for fixed W_1 and W_2 in the Γ–k plane: effect of interfacial tension between the two fluids on the neutral curves. The parameters are: $W_1 = 0.5$, $W_2 = 0.1$, $\beta = 0.4$, $\Sigma = 0.1$, $\eta_r = 0$, $H = 0.7$.

interfacial mode between the two fluids can be stabilized completely. On the other hand, if $W_1 > W_2$ and when the thickness of fluid 2 is smaller, then if the wall is made sufficiently deformable, the interfacial mode between the two fluids becomes unstable. This shows that the effect of the solid layer on the two-fluid purely elastic interfacial mode is qualitatively different from the effect of a third UCM fluid considered by Ganpule and Khomami [6].

3.4. Comparison with the neo-Hookean solid model

In this section, we provide a brief comparison of the results obtained using the linear viscoelastic solid model and the neo-Hookean model. First, we briefly recall the results obtained in earlier studies on the single layer flow of both Newtonian and UCM fluids past a solid layer using the neo-Hookean model, since those results are pertinent to the mode 2 instability for the three-layer configuration of interest in this study. At the outset, one might expect that the linear elastic model, strictly speaking, is valid only when the nondimensional strain in the base state (see Eq. (10)) of the solid layer, Γ, is small compared to 1. However, it was shown by Gkanis and Kumar [21] for Newtonian fluids and by Shankar and Kumar [15] for UCM fluids that for $H \geq 2$, the results obtained using the linear elastic solid model and the neo-Hookean model agreed very well for mode 2, even though the critical strain Γ_c is not strictly small compared to 1. In general, it was found that the Γ_c required to destabilize the flow was smaller for the neo-Hookean model when compared to the linear elastic solid model, and the differences in the predictions of the two solid models diminish as H is increased. Thus, earlier studies have shown that the

results obtained for mode 2 instability are unaffected by the neo-Hookean model for $H \geq 2$. However, the study of Gkanis and Kumar showed that there appears a new instability at somewhat higher wavenumbers for a neo-Hookean solid, which is absent for a linear viscoelastic solid. When $H < 2$, the critical strain (Γ_c) required to destabilize these high wavenumber perturbations are smaller than the Γ_c required to destabilize the $k \sim O(1)$ perturbations that is already predicted by the linear viscoelastic model.

From the point of view of the three-layer configuration of interest in this paper, one must also determine the role of using the neo-Hookean model on mode 1 instability, in order to examine whether the predictions made in the previous sections (using the linear viscoelastic model) are affected by the model used to describe the solid layer. To this end, we have carried out the linear stability analysis using the neo-Hookean model, by adapting the formulation of Gkanis and Kumar [21] to the present three-layer configuration. The reader is referred to [15,21] for details concerning the formulation of the linear stability analysis involving a neo-Hookean solid. Fig. 20 shows a representative comparison of the neutral stability curves (in the Γ–k plane) obtained using the linear viscoelastic solid model with $\eta_r = 0$, and the neo-Hookean model. Let us first focus on the mode 1 neutral curve. As demonstrated in this figure, the neutral curve obtained using the linear elastic solid model agrees quite well with that of the neo-Hookean solid model. There are minor quantitative differences, but the qualitative features are the same for mode 1, and the prediction that mode 1 is stabilized by the solid layer (for $W_2 > W_1$ when $\beta < 1/2$) is hence unaffected by the neo-Hookean model for the solid. For mode 2, however, there is an important difference because for $H < 2$, there is a new high wavenumber instability in the neo-Hookean model that is not captured by the linear viscoelastic model. This high wavenumber instability arises because of the nonzero first normal stress difference that exists in the base state for the neo-Hookean solid (while it is zero in a linear elastic solid). The discontinuity in the first normal stress difference between the UCM fluid 2 and the neo-Hookean solid apparently gives rise to this high wavenumber instability, much similar to the high-k instability between two UCM fluids with different relaxation times. For $H < 2$, the Γ_c required to destabilize these high-k mode 2 perturbations is smaller than that required for the $k \sim O(1)$ instability that is already predicted by the linear viscoelastic model. Therefore, for $H < 2$, one must plot the neutral curve for these high-k perturbations. This is shown in the two plots of Fig. 20. As demonstrated by these plots, the critical Γ_c to destabilize these high-k mode 2 perturbations is still a significantly large quantity, and there remains a window in the Γ–k plane where both the modes are stable. It is therefore expected that the important qualitative conclusions drawn in the previous sections using the linear viscoelastic model should remain unaffected with the use of a more realistic constitutive model for the solid.

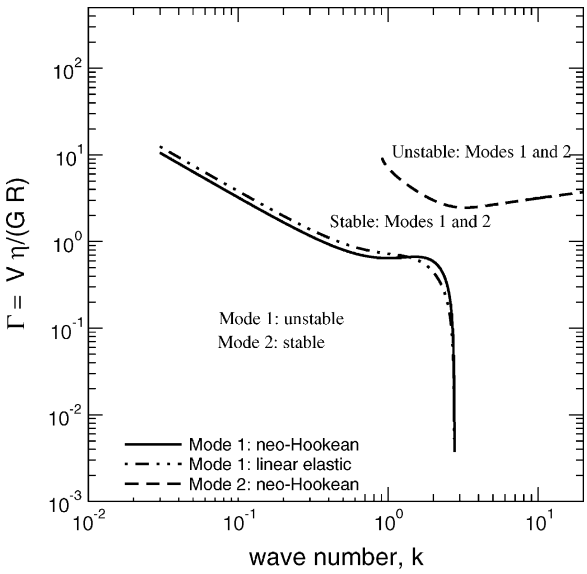

(a) $W_1 = 0.1, W_2 = 0.5, H = 0.7$

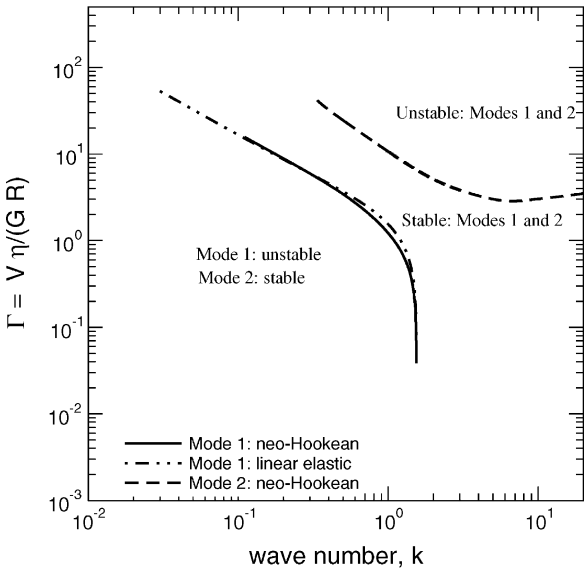

(b) $W_1 = 0.5, W_2 = 0.6, H = 0.3$

Fig. 20. Neutral stability curves for mode 1 and mode 2 instabilities for fixed W_1 and W_2 in the Γ–k plane: comparison of results obtained for the linear viscoelastic model with the results of the neo-Hookean solid. For the neo-Hookean solid, the interfacial tension (σ) between the solid and the UCM fluid 2 is nonzero, with nondimensional value $\sigma/(GR) = 1$. Data for $\beta = 0.4$, $\eta_r = 0$, $\Sigma = 0.1$ in both the figures.

4. Concluding remarks

The stability of the three-layer configuration consisting of two viscoelastic UCM fluids undergoing plane Couette flow past a soft, deformable solid layer was analyzed in the creeping flow regime for the case where the viscosities of the two UCM fluids are matched, while their relaxation times are different. This elasticity stratification leads to an

instability (mode 1) in the creeping flow regime for two-layer Couette flow in rigid-walled channels in the absence of the solid layer. The interface between a single UCM fluid and the solid layer also undergoes an instability (mode 2) when the nondimensional elasticity parameter $\Gamma = V\eta/(GR)$ exceeds a critical value. In the three-layer configuration under consideration in this paper, our results show that the waves in the fluid–fluid and fluid–solid interfaces interact strongly, and this was shown to have dramatic consequences on the purely elastic interfacial instability between the two fluids. When the more elastic fluid is present between the less elastic fluid and the solid layer, the deformability of the solid layer has a stabilizing effect on the mode 1 interfacial instability. In this case, when the thickness of the more elastic fluid is smaller, it was demonstrated that it is possible to completely suppress the mode 1 instability (while it is unstable in rigid-walled channels) by increasing the solid layer deformability, and the nondimensional elasticity parameter Γ required to stabilize the mode 1 instability scales as $\Gamma \sim 1/k$ for $k \ll 1$. Modes with $k \gg 1$ are usually stabilized by the nonzero interfacial tension between the two fluids. In general, increasing the solid layer deformability (Γ) further can destabilize the mode 2 instability. However, by carefully tuning the solid layer thickness H and viscosity ratio η_r, it was shown that the mode 2 instability can also be completely suppressed, and the three-layer configuration can be completely stabilized in finite experimental geometries. When the more elastic fluid of larger thickness lies in between the less elastic fluid and the solid layer, solid layer deformability again renders the mode 1 instability to be completely stable.

In the other configuration where the less elastic fluid is in between the more elastic fluid and the solid layer (i.e., the fluid layers in the previous configuration are interchanged), the role of solid layer deformability is completely reversed, and it has a powerful destabilizing effect on the mode 1 instability. Here, when the more elastic fluid is of larger thickness than the less elastic fluid, such a configuration is stable at long waves in rigid channels. However, increase in solid layer deformability was shown to destabilize mode 1, and the nondimensional elasticity parameter required to render the flow unstable scales as $\Gamma \sim 1/k$ for $k \ll 1$. When the less elastic fluid of larger thickness lies in between the more elastic fluid and the solid layer, increasing layer deformability again has a strong destabilizing effect on mode 1 instability.

The present analysis was restricted to the case where the viscosities of the two UCM fluids are matched, in order to exclusively focus on the effect of solid layer deformability on the instability due to elasticity stratification. However, it is expected that the present results should carry over to the case where there is a viscosity stratification as well. Another approximation made in the present study is the assumption of creeping flow regime, where the inertial effects in the two fluids and the solid are negligible. While this approximation is reasonable in polymer processing applications, it does not capture the instability due to viscosity stratification that occurs even in Newtonian fluids [14] at nonzero Reynolds numbers. Therefore, for UCM fluids with both viscosity and elasticity stratification, apart from the effect of solid layer deformability on elasticity stratification, its effect on combined viscosity and elasticity stratification must be studied in order to make connections with general experimental situations. A more complete analysis including viscosity stratification and fluid inertial effects must involve numerical treatment of the problem, and this will be presented in a future study.

Finally, it is useful to estimate the parameters that would be representative of typical experimental situations, in order to determine when the effects predicted in this study can be realized in experiments. For sake of concreteness, let us consider the parameter set considered in Fig. 15(b). The nondimensional parameter Γ required to stabilize the mode 1 instability increases as $\Gamma \sim 1/k$ for $k \ll 1$. However, experimental studies will involve finite geometries, and in such situations, the minimum allowed wavenumber will be dictated by the system length L, as $k_{\min} = 2\pi R/L$, where R is the total thickness of the two fluids. If we assume $L/R = 100$, then $k_{\min} \approx 0.06$, and the Γ required to stabilize perturbations of this wavenumber (and all k larger than this minimum wavenumber) can be obtained from Fig. 15(b) to be greater than or equal to 5. The Weissenberg number of the fluid 2 in this figure is $W_2 = 2$, and so $\Gamma/W_2 \geq 5/2$. The nondimensional group $\Gamma/W_2 = \eta/(\tau_2 G)$ is independent of the fluid velocity V, and if this group is greater than $5/2$ then mode 1 will be stabilized for this particular experimental geometry with $L/R = 100$ and other parameters such as W_1, W_2, β and H are fixed as in Fig. 15(b). (Since $W_1 < W_2$ for this configuration, Γ/W_1 is also greater than $5/2$.) The shear modulus G of deformable solids such as polymer gels or soft elastomers can be estimated to be 10^4 Pa, while the relaxation time τ_2 of typical polymeric liquids is around 10^{-2} s, and a representative viscosity η of polymeric liquids is around 10^3 N s m^{-2}. Using these estimates, the nondimensional group $\eta/(\tau_2 G) = 10$ which is greater than the theoretically predicted $5/2$. Therefore, these estimates show that the predicted stabilization of mode 1 interfacial instability should be realized in experiments involving two-layer flow of typical polymeric liquids past soft solid layers.

References

[1] Y. Renardy, Stability of the interface in two-layer Couette flow of upper convected Maxwell liquids, J. Non-Newtonian Fluid Mech. 28 (1988) 99–115.
[2] K. Chen, Elastic instability of the interface in Couette flow of two viscoelastic liquids, J. Non-Newtonian Fluid Mech. 40 (1991) 261–267.
[3] Y.-Y. Su, B. Khomami, Purely elastic interfacial instabilities in superposed flow of polymeric fluids, Rheol. Acta. 31 (1992) 413–420.
[4] Y.-Y. Su, B. Khomami, Interfacial stability of multilayer viscoelastic fluids in slit and converging channel die geometries, J. Rheol. 36 (1992) 357–387.

[5] H.J. Wilson, J.M. Rallison, Short wave instability of co-extruded elastic liquids with matched viscosities, J. Non-Newtonian Fluid Mech. 72 (1997) 237–251.
[6] H. Ganpule, B. Khomami, A theoretical investigation of interfacial instabilities in the three layer superposed channel flow of viscoelastic fluids, J. Non-Newtonian Fluid Mech. 79 (1998) 315–360.
[7] H. Ganpule, B. Khomami, An investigation of interfacial instabilities in the superposed channel flow of viscoelastic fluids, J. Non-Newtonian Fluid Mech. 81 (1999) 27–69.
[8] S. Scotto, P. Laure, Linear stability of three-layer Poiseuille flow for Oldroyd-B fluids, J. Non-Newtoian Fluid Mech. 83 (1999) 71–92.
[9] G.M. Wilson, B. Khomami, An experimental investigation of interfacial instabilities in the multilayer flow of viscoelastic fluids. Part I. Incompatible polymer systems, J. Non-Newtonian Fluid Mech. 41 (1992) 355.
[10] G.M. Wilson, B. Khomami, An experimental investigation of interfacial instabilities in the multilayer flow of viscoelastic fluids. Part II. Elastic and nonlinear effects in incompatible polymer systems, J. Rheol. 37 (1993) 315.
[11] G.M. Wilson, B. Khomami, An experimental investigation of interfacial instabilities in the multilayer flow of viscoelastic fluids. Part III. Compatible polymer systems, J. Rheol. 37 (1993) 341.
[12] B. Khomami, G.M. Wilson, An experimental investigation of interfacial instabilities in the superposed flow of viscoelastic fluids in converging/diverging channel geometry, J. Non-Newtonian Fluid Mech. 58 (1995) 47.
[13] M. Gad-el-hak, Drag reduction using compliant walls, in: P.W. Carpenter, T.J. Pedley (Eds.), IUTAM Symposium on Flow Past Highly Compliant Boundaries and in Collapsible Tubes, Kluwer Academic Publishers, 2003, Chapter 9, pp. 191–229.
[14] C.S. Yih, Instability due to viscosity stratification, J. Fluid. Mech. 27 (1967) 337–350.
[15] V. Shankar, S. Kumar, Instability of viscoelastic plane Couette flow past a deformable wall, J. Non-Newtonian Fluid Mech. 116 (2004) 371.
[16] R.G. Larson, Constitutive Equations for Polymer Melts and Solutions, Butterworths, Boston, 1988.
[17] V. Kumaran, G.H. Fredrickson, P. Pincus, Flow induced instability of the interface between a fluid and a gel at low Reynolds number, J. Phys. II France 4 (1994) 893–904.
[18] V. Kumaran, Stability of the viscous flow of a fluid through a flexible tube, J. Fluid. Mech. 294 (1995) 259–281.
[19] V. Shankar, V. Kumaran, Stability of non-parabolic flow in a flexible tube, J. Fluid. Mech. 395 (1999) 211–236.
[20] V. Shankar, V. Kumaran, Stability of fluid flow in a flexible tube to non-axisymmetric disturbances, J. Fluid. Mech. 408 (2000) 291–314.
[21] V. Gkanis, S. Kumar, Instability of creeping Couette flow past a neo-Hookean solid, Phys. Fluids. 15 (2003) 2864–2871.
[22] V.A. Gorodtsov, A.I. Leonov, On a linear instability of plane parallel Couette flow of viscoelastic fluid, J. Appl. Math. Mech. 31 (1967) 310–319.